Simulated delay in the onset of the rainy season in Central East Brazil under global warming influenced by plant physiological response

Jerry B Samuel,[a] Marcia T. Zilli,[a] Neil C. G. Hart,[a] Kate Halladay,[b] Ron Kahana,[b] Robin Chadwick,[b,c] Sonja Folwell,[d]

[a] *School of Geography and the Environment, University of Oxford, S Park Rd, Oxford, OX13QY, Oxfordshire, United Kingdom.*

[b] *Met Office, FitzRoy Rd, Exeter, EX1 3PB, Devon, United Kingdom*

[c] *Global Systems Institute, Department of Mathematics and Statistics, University of Exeter, United Kingdom*

[d] *UK Centre for Ecology and Hydrology, Wallingford, OX10 8BB, Oxfordshire, United Kingdom*

Corresponding author: Jerry B Samuel, jerry.samuel@ouce.ox.ac.uk

Early Online Release: This preliminary version has been accepted for publication in *Journal of Climate*, may be fully cited, and has been assigned DOI 10.1175/JCLI-D-24-0720.1. The final typeset copyedited article will replace the EOR at the above DOI when it is published.

ABSTRACT: The projected delay in the onset of the South American monsoon over Central East Brazil under global warming is explored in a pair of convection-permitting regional climate model (CPRCM) simulations performed at the UK Met Office, corresponding to the present day and an RCP8.5 scenario. We also examine the corresponding driving general circulation model (GCM) simulations to understand the impact of explicitly resolving convection within the CPRCM. The transition to the rainy season is associated with the buildup of lower tropospheric moist static energy and moisture, the demands for which are enhanced in the RCP8.5 scenario. However, significant reductions in evapotranspiration and the absence of moisture flux convergence enhancement in September and October renders unfavorable conditions for the onset of the rains in the future climate. The reduced evapotranspiration is irrespective of an increase in column soil moisture in the RCP8.5 scenario. A stomatal response to altered environmental conditions in the future climate contributes to this decline in evapotranspiration. These changes lead to a delayed and more abrupt onset in the RCP8.5 scenario. The direction of change in the onset is similar in both the CPRCM and the driving GCM, although the CPRCM is drier than the GCM during the onset phase. The findings from this study highlight the role of plant physiology in modulating climate projections and the necessity to improve their representation in climate models.

Accepted for publication in *Journal of Climate*. DOI 10.1175/JCLI-D-24-0720.1.

SIGNIFICANCE STATEMENT: Optional significance statement goes here.

1. Introduction

In austral summer, large swathes of tropical and subtropical South America come under the influence of the South American Monsoon System (SAMS). During the pre-monsoon and early monsoon season, spanning September to November, the rains migrate from northern South America to locations in central and southeast Brazil (Gan et al. 2004; Vera et al. 2006). Several criteria exist to identify the onset of SAMS and the associated increase in precipitation (e.g., Kousky 1988; Gan et al. 2005; da Silva and de Carvalho 2007; Raia and Cavalcanti 2008; Bombardi et al. 2019), although the spatial pattern of the progression of onset can vary depending on the onset criteria used (Bombardi et al. 2020). In general, the rainy season begins first in the regions to the south of Amazon and Southeast Brazil between August and October, while it occurs last in northeast Brazil (Kousky 1988; Liebmann et al. 2007). In Central Brazil, the onset of the rainy season happens in the second half of October, but it can vary from late September to early November, indicating significant interannual variability (Marengo et al. 2012). Such early or late onsets are associated with significant changes in the moisture flux convergence and atmospheric circulation (Talamoni et al. 2022; Espinoza et al. 2021).

Both local land surface processes and remote oceanic teleconnections have been linked to the onset variability. Studies have shown that surface warming during the dry-to-wet transition coupled with the moisture availability in the region enables the atmosphere to overcome convective inhibition and initiate the rainy season (Fu et al. 1999; Smyth and Ming 2021). Cold fronts, and associated upper-level waves could play a role here by providing favorable conditions for the onset and the establishment of the South Atlantic convergence zone (SACZ) (Nieto-Ferreira et al. 2011). SACZ is a prominent feature of the rainy season, recognizable as a northwest-southeast oriented region of convergence situated to the west of the subtropical South Atlantic high and to the east of the Chaco low (Kodama 1992), with its location influenced by the topography in central-east Brazil (Marengo et al. 2012). The SACZ is associated with significant low-level moisture convergence and rainfall (de Oliveira Vieira et al. 2013), and its formation marks a regime transition in the region's dynamics (Nieto-Ferreira et al. 2011).

Accepted for publication in *Journal of Climate*. DOI 10.1175/JCLI-D-24-0720.1.

The importance of land-atmosphere interactions in the transition zones between dry and wet climates has been highlighted in previous studies (Koster et al. 2004). Several monsoon regions have been identified as areas with significant land-atmosphere coupling, particularly in the post-monsoon season (Dirmeyer et al. 2009). In the context of SAMS, rainfall during the dry-to-wet transition period from September to November also shows strong sensitivity to land processes (Wei and Dirmeyer 2012; Baker et al. 2021). Studies have shown that early onset of the rainy season in South Amazon is associated with wetter soil conditions and increased latent heat flux (Fu and Li 2004; Collini et al. 2008). Wet soil can act as a moisture source, contributing to precipitation recycling, with its relative importance varying spatially (Martinez and Dominguez 2014; Zemp et al. 2014; Zanin and Satyamurty 2021). The evaporation from the land surface aids in destabilizing the atmosphere thereby supporting the development of deep convection (Lintner and Neelin 2009; Wright et al. 2017; Smyth and Ming 2021). Drier soil, on the other hand, has been shown to delay the onset possibly due to a drier boundary layer and reduced convective available potential energy (Collini et al. 2008).

Vegetation and land cover type play a significant role in controlling land evaporation (Gash and Nobre 1997), which in turn can change the surface energy partitioning and boundary layer characteristics (Eltahir 1998; Findell and Eltahir 2003). Numerical experiments using GCMs have shown that vegetation processes can modulate the onset of the rainy season in South America (e.g., Xue et al. 2006). Vegetation changes can alter Bowen ratio and gradients of moisture and moist static energy that can influence the progress of onset. Over southern Amazon, transpiration aids in the development of deep convection by moistening the atmosphere via shallow convection during the onset of rainy season (Wright et al. 2017). Moisture variability in the Amazon rainforest can also modulate the rainfall in southern parts of Brazil via changes in moisture transport (Martinez and Dominguez 2014; Zanin and Satyamurty 2021; Bottino et al. 2024).

The role of altered land-atmosphere feedbacks including plant physiological response to increases in temperature and CO_2 therefore need to be explored, since studies suggest that these processes influence precipitation characteristics over land (Andrews et al. 2011; Miralles et al. 2019). Uncertainties in modelling these processes can lead to significant variability in climate projections (Jia et al. 2019). The robustness of these projections is also limited by the uncertainty in the projected changes in the Pacific sea surface temperature (Seager et al. 2019; Cai et al. 2021), which can

Accepted for publication in *Journal of Climate*. DOI 10.1175/JCLI-D-24-0720.1.

impact global teleconnections. In addition, since SAMS onset can also be influenced by Atlantic SSTs (Bombardi and Carvalho 2011), future projections of Atlantic SSTs also need to be improved (Nworgu et al. 2024). Despite these modelling challenges, there is growing consensus that SAMS onset will be delayed under global warming (Moon and Ha 2020; Thome Sena and Magnusdottir 2020; Ashfaq et al. 2021; Agudelo et al. 2023). The CMIP6 ensemble also consistently demonstrates a trend towards early summer drying (Douville et al. 2021). Furthermore, the projected delay in SAMS is also supported by observed trends in the past century (Fu et al. 2013; Correa et al. 2021; Espinoza et al. 2021). Correa et al. (2021) found a significant trend towards delayed onsets in Southern Amazon and southeast Brazil. The dry season is also drying further with more dry days observed in the south and east Amazon (Haghtalab et al. 2020). The Cerrado region of Brazil has also experienced a reduction in rainfall during the wet season onset (Hofmann et al. 2023). Marengo et al. (2022) demonstrated that a delayed wet season onset over Cerrado and the associated increase in near surface temperature and vapour pressure deficit raised the probability of occurrence of compound drought-heat extremes.

Kilometer-scale convection-permitting regional climate models (CPRCMs), with improved representation of orography and land heterogeneity as well as explicit simulation of deep convection, can provide a better representation of various processes linking land surface and rainfall (Hohenegger et al. 2009; Kendon et al. 2012; Prein et al. 2015; Stratton et al. 2018; Rowell and Berthou 2023). This enhances the potential of CPRCMs to better capture the interaction between convective initiation and mesoscale processes such as soil moisture-precipitation feedbacks (Taylor et al. 2013), which is known to be of significance in South America (Baidya Roy and Avissar 2002; Chug et al. 2023). The representation of the diurnal cycle and the frequency distribution of precipitation also show significant improvement in CPRCM simulations (Halladay et al. 2023).

In the present study, CPRCM simulations over South America (Halladay et al. 2023; Kahana et al. 2024) are used to examine changes in the onset of the rainy season over Central East Brazil in a global warming scenario. The paper is organized as follows: Section 2 describes the model and data description, Section 3 describes the seasonal cycle of major hydrological parameters over the region, Section 4 discusses the processes involved in the onset of the rainy season, Section 5 examines the changes in the moisture budget during the onset, Section 6 analyzes the role of

Accepted for publication in *Journal of Climate*. DOI 10.1175/JCLI-D-24-0720.1.

vegetation during the onset, Section 7 evaluates the implications for land-atmosphere coupling, and Section 8 provides the major conclusions.

2. Data, model description, and study region

The CPRCM used here is a configuration of the Met Office Unified Model (UM) version 10.6 with a horizontal grid resolution of 4.5 km and 80 vertical levels, with 32 levels below 5 km. At this spatial resolution, the convection parametrization is turned off and the convection can be explicitly simulated, even though the smaller-scale convection is still not resolved. Two 10-year long simulations performed using the CPRCM are examined in this study. The first, termed CPRCM-PD, is the present-day simulation with lateral boundary conditions (LBCs) derived from a UK-Met Office global atmosphere-land GCM simulation at 25 km resolution (MOHC-HadGEM3-GA7GL-N512), forced by observed sea surface temperature (SST) and sea ice (Reynolds et al. 2007). The present-day CPRCM simulation is performed for the years 1998-2007 and has a time varying green house gas concentration corresponding to that period. The second experiment, CPRCM-2100, corresponds to the high-emission RCP8.5 scenario, which takes into account changes in greenhouse gases and sea surface temperatures (SSTs) while excluding changes in land use and aerosols. In this simulation, changes in monthly SST between present and future simulations from the Met Office Hadley Centre Global Environmental Model version 2 with Earth System components (HadGEM2-ES) RCP8.5 simulation are added to the observed SST and sea ice dataset and then used to force the 25km GCM future simulation. More details on the design of experiments are given in Halladay et al. (2023) and Kahana et al. (2024). In addition to the CPRCM simulations, we also examine the corresponding driving GCM simulations to understand the impact of explicitly resolving convection (these GCM experiments are termed GCM-PD and GCM-2100). The GCM runs have a horizontal resolution of 25 km and 85 vertical levels, with 26 levels below 5 km. A parametrization scheme based on Gregory and Rowntree (1990) is used in the GCM to represent convection.

The land surface processes in these experiments are represented using Joint UK Land Environment Simulator (JULES) (Best et al. 2011). The soil column is 3m deep and has four soil layers of depth 0.1, 0.25, 0.65, and 2m. It has nine land cover types consisting of five plant functional types (PFTs: broadleaf tree, needle leaf tree, C3 grass, C4 grass, and shrub) and four non-vegetation

Accepted for publication in *Journal of Climate.* DOI 10.1175/JCLI-D-24-0720.1.

tiles (urban areas, inland water, bare soil, and land ice). C4 grasses, found in warmer tropical regions employs a more efficient photosynthetic pathway that minimizes photorespiration. JULES accounts for this and employs different photosynthetic pathways for C3 and C4 grasses as mentioned in Clark et al. (2011). Vegetation root density decays exponentially with soil depth and is a function of PFT. Only the broadleaf PFT has significant access to moisture in the bottommost soil layer in the study region. A brief description about the parametrization of soil water uptake by vegetation in JULES is given in the Supplementary file. The land cover fraction is the same in both the present-day and RCP8.5 simulations.

The present study focuses on Central East Brazil (CEB: $20°S - 5°S, 60°W - 40°W$; shown in Figure 1a), which encompasses regions noted in the IPCC AR6 to experience a delay in the onset of the rainy season due to increases in greenhouse gases (Douville et al. 2021; Correa et al. 2021; Debortoli et al. 2015; Ashfaq et al. 2021; Bombardi and Boos 2021). The vegetation in this region consists primarily of broadleaf trees, C4 grass, and C3 grass (Figure 1 a-d), although their distribution is uneven. Broadleaf trees are found in the northwestern areas of CEB while C3 grass and C4 grass are found elsewhere in CEB. To account for this diversity in land cover distribution and the differing rainfall characteristics, we have subdivided this CEB region into West CEB (WCEB: $14°S - 5°S, 60°W - 50°W$), East CEB (ECEB: $14°S - 5°S, 50°W - 40°W$), and South CEB (SCEB: $20°S - 14°S, 60°W - 40°W$), and report subregional differences when notable. All data are regridded to parent model resolution of 25 km using a first-order conservative area-weighted regridding scheme for ease of analysis.

The CPRCM-PD's ability to simulate the climate over South America with reasonable skill has been demonstrated by Halladay et al. (2023), despite having a tendency to produce more dry days and heavier rainrates than the driving GCM-PD. The CPRCM-PD reduces the wet bias in annual precipitation over central Brazil compared to the GCM-PD (Halladay et al. 2023). CPRCM-PD also simulate some of the major features of the SAMS, like the cloud band events and the SACZ, with reasonable accuracy (Zilli et al. 2024). A detailed discussion on the CPRCM-PD's performance over South America can be found in the above mentioned references. Future projections of rainfall from CPRCM-2100 suggest an increase in precipitation intensity and extremes (Kahana et al. 2024).

Accepted for publication in *Journal of Climate*. DOI 10.1175/JCLI-D-24-0720.1.

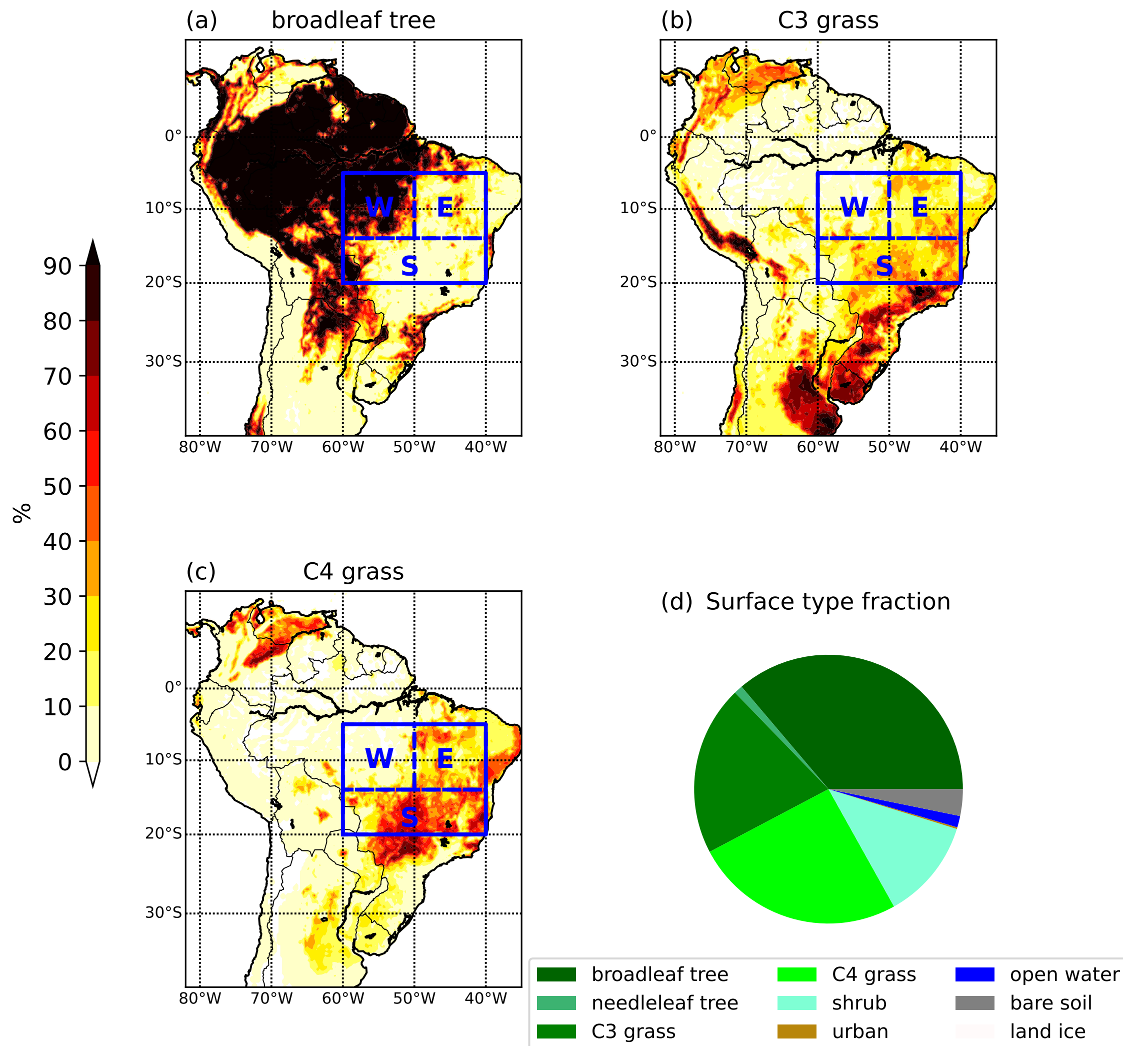

FIG. 1. Land cover types in the experiments. Percentage of area occupied by (a) broadleaf tree, (b) C3 grass, (c) C4 grass. (d) Fraction of area occupied by different surface types in CEB (region marked by the blue box in panel a-c. The dashed blue lines inside CEB represents the subregions WCEB, ECEB, and SCEB, which are indicated by W, E, and S, respectively, in panels a-c.

The study uses daily rainfall data from IMERG (v07B) (Huffman et al. 2024) and ERA5 (Hersbach et al. 2020) for comparison of simulated rainfall. Thermodynamic variables like temperature, geopotential, and specific humidity are compared against ERA5 .

Accepted for publication in *Journal of Climate*. DOI 10.1175/JCLI-D-24-0720.1.

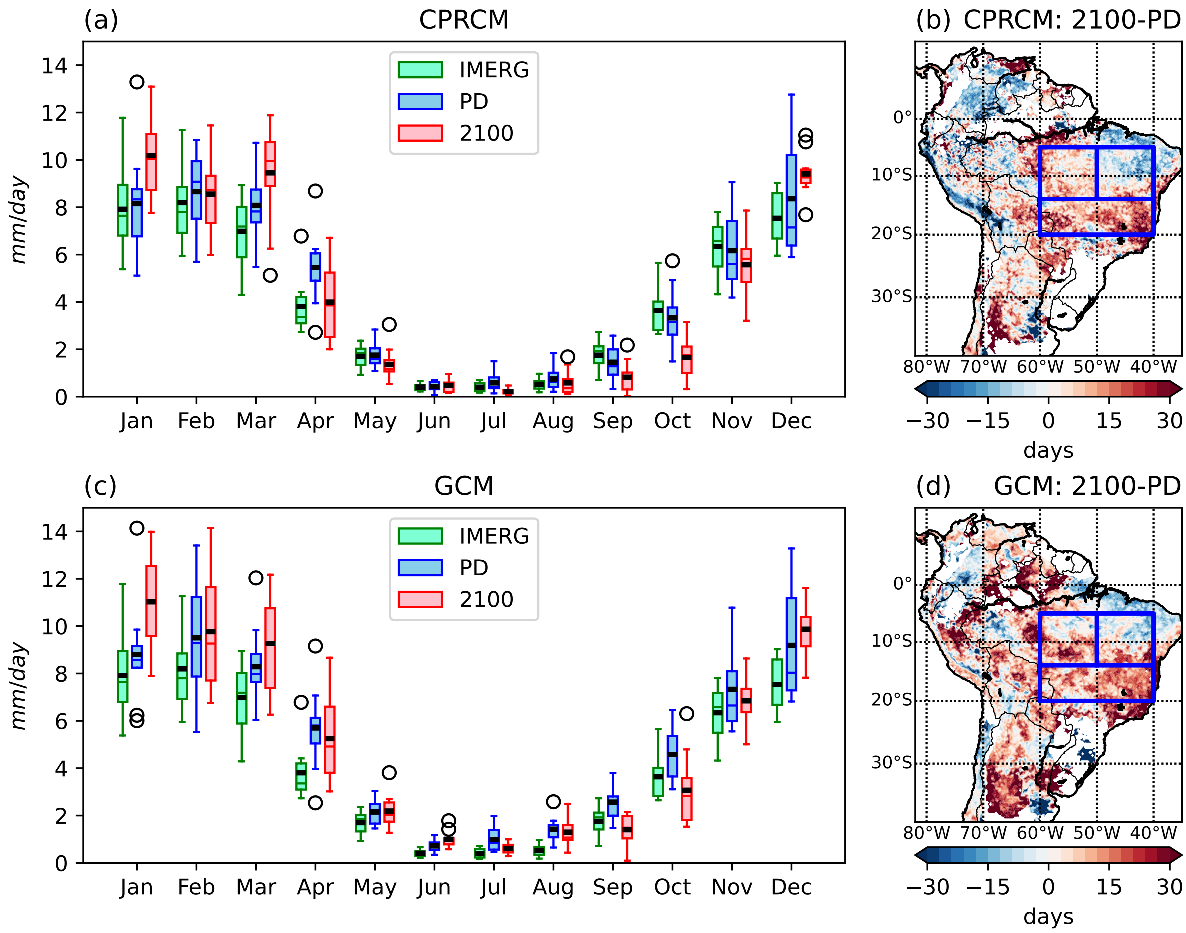

FIG. 2. Rainfall and onset dates. (a) Seasonal cycle of rainfall over CEB in IMERG, CPRCM-PD, and CPRCM-2100, (b) Difference in rainy season onset dates between CPRCM-2100 and CPRCM-PD, (c) seasonal cycle of rainfall over CEB in IMERG, GCM-PD, and GCM-2100, and (d) Difference in rainy season onset dates between GCM-2100 and GCM-PD. The box limits in panels a,c show the inter quartile range. The horizontal line (green, blue or red) within the box (green, blue or red) represents the median and the black line shows the mean. The whiskers extend till the farthest data point lying within 1.5 times the inter-quartile range from the box.

3. Seasonal cycle of rainfall

The seasonal cycles of precipitation over CEB in the observation and the simulations are shown in Figure 2a,c. The simulated seasonal cycle for the present-day compares well with IMERG rainfall data, with the CPRCM performing better than the GCM, especially during the onset phase. Precipitation starts to increase in September, marking the transition towards the onset of the rainy season, the peak of which is in December through January. The CEB region has a large decline

Accepted for publication in *Journal of Climate*. DOI 10.1175/JCLI-D-24-0720.1.

in rainfall during this transition season, suggesting a possible delay in rainfall onset (Figure 2a,c). Rainfall decline is also observed over the Amazon whereas rainfall increases in south Brazil (see Supplementary Fig. 1 for map of percentage change). The mean onset dates over CEB, computed using the method of Bombardi et al. (2019), are November 4 and October 24 for CPRCM-PD and GCM-PD. According to this method, the onset of the rainy season is indicated by the inflection point of the accumulated precipitation anomaly timeseries corresponding to an increase in precipitation, although this may involve more intricacies as mentioned in their paper. Despite similar seasonality in the RCP 8.5 scenario, there are significant changes during the onset period and the peak rainy season. In both the CPRCM and the GCM simulations, the onset of precipitation is delayed by almost a month with a significant increase in precipitation happening only from October under the RCP 8.5 scenario (Figure 2a,c). Nevertheless, precipitation increases rapidly thereafter, reaching present-day values by December and exceeding the present-day values in January and March. This delay in the onset of the rainy season for the future scenario is quite large in CEB, particularly in SCEB and WCEB; Eastern Amazon and parts of central and subtropical South America also experience some delay (Figure 2b, d).

4. Thermodynamics of rainy season onset

The onset of the rainy season is marked by coherent changes in precipitation and the thermodynamic structure of the atmosphere. Figure 3 summarises the evolution of precipitation and three thermodynamic quantities, namely moist static energy (MSE), dry static energy (DSE), and moisture over CEB during the onset phase for the present-day and future in both models. Here MSE and DSE are given by,

$$MSE = C_p T + gZ + Lq, \tag{1}$$

$$DSE = C_p T + gZ, \tag{2}$$

where C_p is specific heat capacity of dry air (1005 J/kg/K), T is the air temperature, g is the acceleration due to gravity (9.81 m/s), Z is the geopotential height, L is the latent heat of vaporization of water (2.501x10^6 J/kg), and q is the specific humidity. The contours of MSE, DSE and moisture are plotted after subtracting the corresponding climatological value in August to highlight the

Accepted for publication in *Journal of Climate*. DOI 10.1175/JCLI-D-24-0720.1.

evolution of these quantities from pre-onset conditions (in general, MSE, DSE and Lq are higher throughout the entire troposphere in the RCP8.5 scenario). The green lines in Figure 3 show the simulated daily mean rainfall (smoothed by a 5-point running mean) from September 1^{st} to November 20^{th} in the present-day (Figure 3d-f for the CPRCM and Figure 3j-l for the GCM) and future simulations (Figure 3g-i for the CPRCM and Figure 3m-o for the GCM). In the present-day, rainfall is simulated to increase in two stages; an increase in the second half of September and then a further increase in early November. The simulated evolution of rainfall compares well with the IMERG dataset which also exhibits a two-stage increase in rainfall, despite differences in magnitude (Figure 3a-c). In the simulations, the second stage of rainfall increase is slightly late compared to that of the observations. In contrast, in the future RCP8.5 scenario, the first stage of rainfall increase in September is absent, and the rainfall increase happens more abruptly in late October or early November.

Previous studies on monsoons (e.g., Chakraborty et al. 2006) have shown that the onset of the rainy season is associated with the accumulation of low-level MSE, which could help explain the differences in the onset of the rainy season in CEB in the present-day and future simulations. Figure 3 (left column) shows the evolution of MSE in the troposphere during the dry-to-wet transition in CEB. In the present-day, similar to the increase in precipitation, low- and mid-troposphere MSE mainly increase in two stages, one in late September and another in early November (Figure 3 d,j) and the simulations compare well with observation (Figure 3a). In the RCP8.5 simulations, the MSE increase starts only around mid-October, followed by an abrupt increase around early November (Figure 3 g,m). The relative increase in MSE required to reach a similar precipitation rate is also larger in the RCP8.5 scenario compared to present-day. This is partly due to the the smaller relative humidity in the warmer future scenario (not shown). The close association between the low-level MSE and precipitation evolution provide a diagnostic explanation for the delayed onset in the future scenario.

Futher insight can be obtained by partitioning the MSE into contributions from DSE and moisture (Lq) (Figure 3 second and third columns, respectively). As for MSE, here DSE and Lq are also relative to August's climatology. The major contribution to low-level MSE increase during the dry-to-wet transition comes from the increase in Lq (Figure 3, third column). The moisture content increases gradually through the dry-to-wet transition in the present day and more abruptly in the

Accepted for publication in *Journal of Climate*. DOI 10.1175/JCLI-D-24-0720.1.

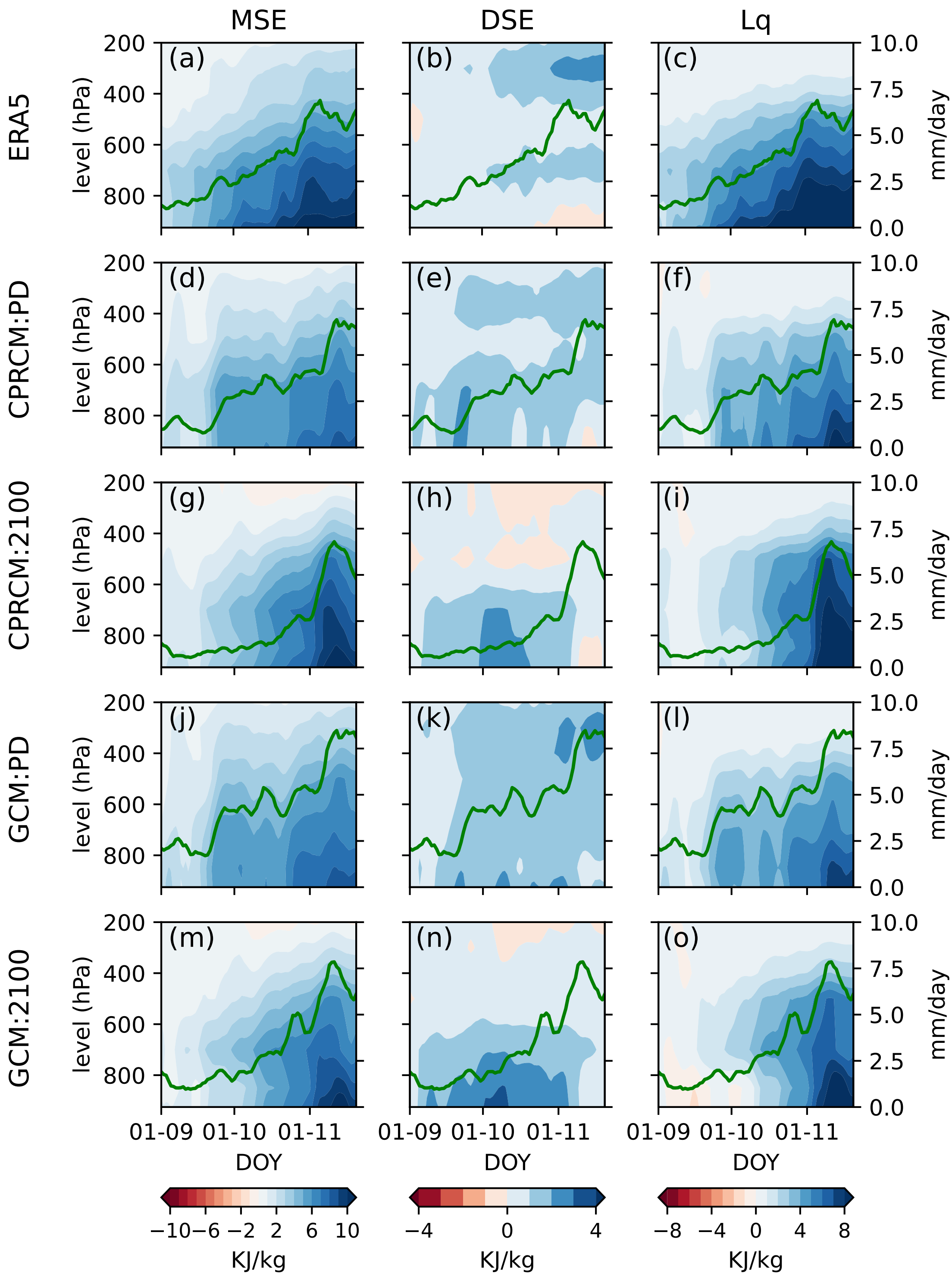

FIG. 3. MSE (left column), DSE (middle column), and Lq (right column) evolution over CEB in ERA5 (a-c), CPRCM-PD (d-f), CPRCM-2100 (g-i), GCM-PD (j-l), and GCM-2100 (m-o). Green lines in each panel represent precipitation (IMERG precipitation is plotted in panels a-c). MSE, DSE, and Lq values are plotted relative to corresponding climatological mean August values to show the build-up of these quantities during the onset phase with the same scale in both present-day and future simulations.

Accepted for publication in *Journal of Climate*. DOI 10.1175/JCLI-D-24-0720.1.

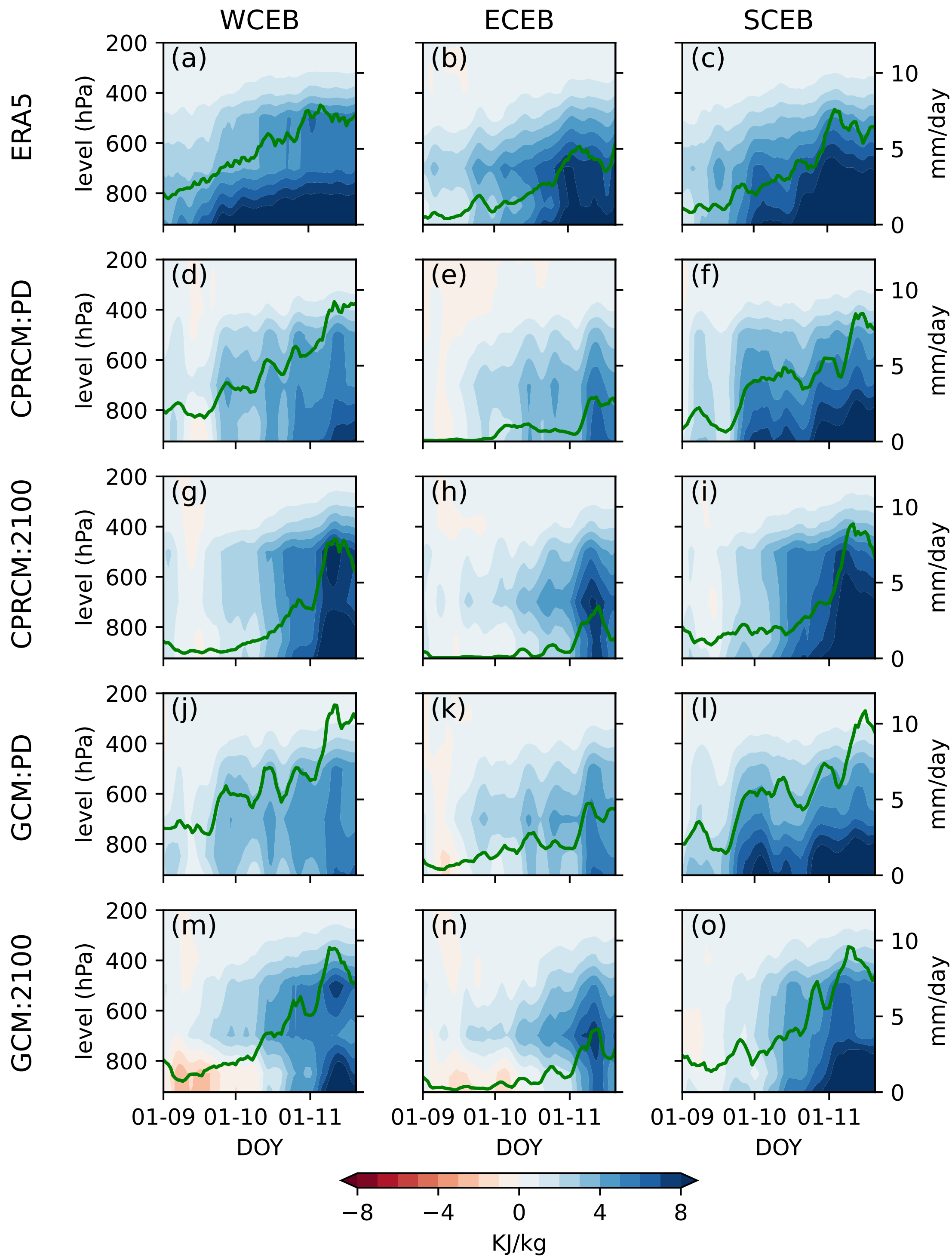

FIG. 4. Lq evolution (relative to corresponding climatological mean August values) over WCEB (left column), ECEB (middle column), and SCEB (right column) in ERA5 (a-c) CPRCM-PD (d-f), CPRCM-2100 (g-i), GCM-PD (j-l), and GCM-2100 (m-o). Green lines represent precipitation (precipitation in panels a-c is based on IMERG dataset). See Figure 1b for the location of each subregion.

Accepted for publication in *Journal of Climate*. DOI 10.1175/JCLI-D-24-0720.1.

future scenario, in agreement with the MSE increase and the onset of precipitation. However, the relative increase in moisture in the observation is larger than in the simulations (Figure 3c). Additionally, a relatively larger future increase (RCP 8.5 - Present-day) in DSE in the upper troposphere (increases by $\approx 13KJ/kg$) compared to the lower troposphere (increases by $\approx 7.5KJ/kg$), suggests a larger dry static stability (defined as the difference in DSE between the upper troposphere and lower troposphere, $DSE_{200} - DSE_{925}$) in the RCP8.5 scenario (see Supplementary Figure 2). In this scenario, a larger build-up of moisture in the lower troposphere is required for the destabilization of the atmosphere. Such increases in dry static stability and boundary layer moisture have been reported in other studies as well (e.g. Seth et al. 2013).

The observed multistage increase in rainfall and the associated thermodynamic variables could reflect a composite signal of onset from different subregions within CEB which can have onset timing differences of up to a month. We consider this possibility by analyzing the evolution of these parameters separately for each subregion as shown in Figure 4. In the present-day simulations, the increase in atmospheric humidity (and consequently precipitation) starts around early October in both WCEB and SCEB (Fig 4 d,g,j,m and f,i,l,o), while in ECEB the transition happens in November (Fig 4 e,h,k,n). The simulated Lq evolution is similar to that in ERA5 (Fig 4b-c) over both ECEB and SCEB where precipitation exhibits a multistage increase. However, over WCEB, a more gradual increase in Lq and precipitation is observed in ERA5 compared to the simulations (Fig 4a). In the RCP8.5 scenario, the atmospheric moisture build-up during October is either absent (CPRCM-2100) or subdued (GCM-2100) in both WCEB and SCEB and the rainfall increase in November is associated with a larger relative increase in atmospheric moisture content compared to present-day. Over ECEB, the rainfall increase in the RCP8.5 scenario happens almost around the same time as in the present day (early November), although with a requirement for larger amounts of atmospheric moisture.

Previous studies have shown that precipitation increases exponentially with increase in atmospheric moisture content (Bretherton et al. 2004). Consistent with these findings, daily mean precipitation over CEB exhibits an exponential relationship with daily-mean low-level specific humidity during the onset phase over CEB (we have taken the specific humidity at 925 hPa as an indicator of atmospheric moisture content) in the present-day simulations (Figure 5b,c). Such an exponential relationship is visible in the observations as well (Figure 5a). The exponential rela-

Accepted for publication in *Journal of Climate.* DOI 10.1175/JCLI-D-24-0720.1.

tionship is maintained in the RCP8.5 scenario as well, but the curve extends to the right indicating the need for higher low-level specific humidity in the future to achieve the same rainfall intensities as the present. In addition, the smallest daily-mean specific humidity values in Figure 5b,c are of similar magnitudes in both the present-day and future simulations, especially in the GCM, possibly enhancing the moisture buildup required for significant rainfall to begin. This is akin to the upped-ante mechanism described in Chou and Neelin (2004) in that the warmer and drier (from a relative humidity perspective) pre-onset conditions demand larger low-level moisture to overcome the enhanced atmospheric stability. The role of boundary layer moisture in determining precipitation change has also been discussed in Chou et al. (2009), Chadwick et al. (2013) and Ma et al. (2018). The rate of increase of precipitation with specific humidity is also marginally lower in the RCP8.5 scenario indicating reduced sensitivity of rainfall to near-surface specific humidity, in addition to an increased variability in absolute moisture content.

There are some differences between the GCM and the CPRCM in the precipitation-moisture relationship. The GCM has larger low-level specific humidity than the CPRCM for similar daily rainfall rates. For instance, the specific humidity corresponding to a rainfall rate of 5mm/day are CPRCM-PD: 12.2g/kg, CPRCM-2100: 15.6g/kg, GCM-PD: 13g/kg, and GCM-2100 16.1g/kg. This larger specific humidity in the GCM is probably linked to the larger frequency of relatively less intense rainfall events in the GCM. However, the exponential relationship in the GCM is closer to that in the observation/reanalysis (Figure 5a). Despite the differences, both the CPRCM and the GCM indicate larger moisture demand for the onset of rainfall in the future scenario. This extra moisture has to be met either by changes in moisture flux convergence or increased evapotranspiration from the land. In the next section, we examine the changes to the moisture budget to investigate this further.

5. Changes to atmospheric moisture budget

To better understand the changes in the hydrological cycle of the atmosphere that lead to the delayed onset of the rainy season, we employ the moisture budget equation given below.

$$\underbrace{\int_{925}^{200} \frac{\partial q}{\partial t} dp/g}_{storage} + \underbrace{\int_{925}^{200} \nabla \cdot (qv) dp/g}_{\substack{\text{Moisture flux} \\ \text{divergence}}} = \underbrace{E}_{evapotranspiration} - \underbrace{P}_{Precipitation} . \tag{3}$$

Accepted for publication in *Journal of Climate*. DOI 10.1175/JCLI-D-24-0720.1.

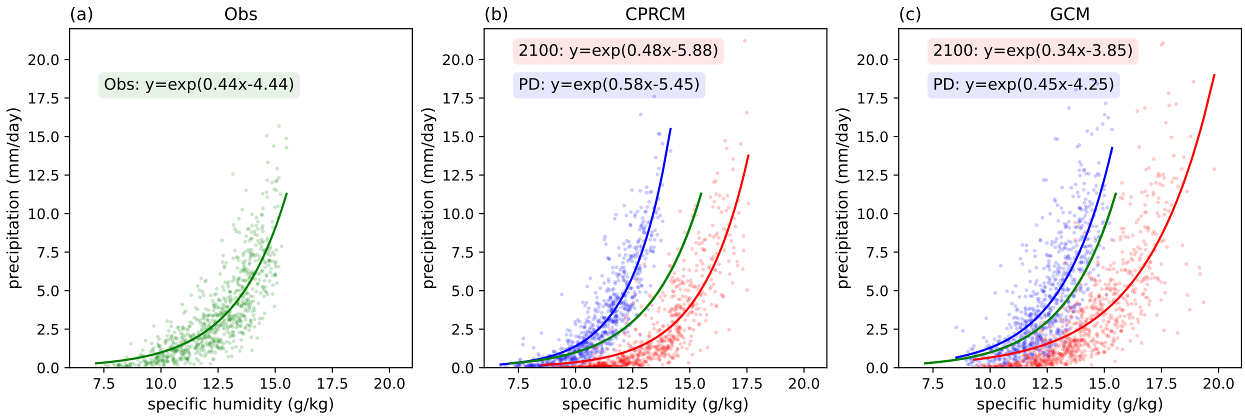

FIG. 5. Relationship between precipitation and specific humidity at 925 hPa over CEB during September 1^{st} to November 20^{th} in (a) observation (specific humidity is from ERA5 and precipitation is from IMERG), (b) CPRCM, and (c) GCM. Blue dots represent present-day simulations and red dots represent RCP8.5 simulations in panels (b) and (c), respectively. The solid lines in each panel show the fitted exponential relationship, with the observed relationship in panel (a) replotted in panels (b) and (c) for comparison.

Here, q is the specific humidity, v is the velocity vector, E is the evapotranspiration, and P is the precipitation. The first term gives the rate of change of column-integrated atmospheric moisture content (between 925 hPa and 200 hPa, represented by $\int$) and represents the storage of water vapour (st). The second term is the horizontal moisture flux divergence (horizontal moisture flux convergence (MFC) is the negative of this term). Here, we estimate MFC as the residual given by $MFC = P - [E - (\partial q/\partial t)]$. In this study, these terms are represented in units of mm/day.

Figure 6a shows the monthly climatology of each term in Equation 3 for CEB. In the present-day, the transition from the dry season ($P - E < 0$) to the wet season ($P - E > 0$) occurs in September when the MFC also becomes positive. The results in Figure 6a also suggest that the differences in the precipitation rate in the CPRCM-PD compared to the GCM arise mainly from the differences in E (compare solid and dotted lines) while the climatology of MFC is similar in the two simulations. The seasonal cycles of rainfall and evapotranspiration are reasonably well captured by the models (a brief discussion on moisture budget in observations is given in the Supplementary File). We now proceed with analyzing how these parameters have changed in the future scenario.

In the CPRCM-2100 simulation, evapotranspiration decreases during the onset phase (Figure 6b), with the greatest reduction ($\approx 40\%$) occurring in October. GCM-2100 experiment shows a larger decline in evapotranspiration than the CPRCM (Figure 6 c). Zanin and Satyamurty (2021) showed

Accepted for publication in *Journal of Climate*. DOI 10.1175/JCLI-D-24-0720.1.

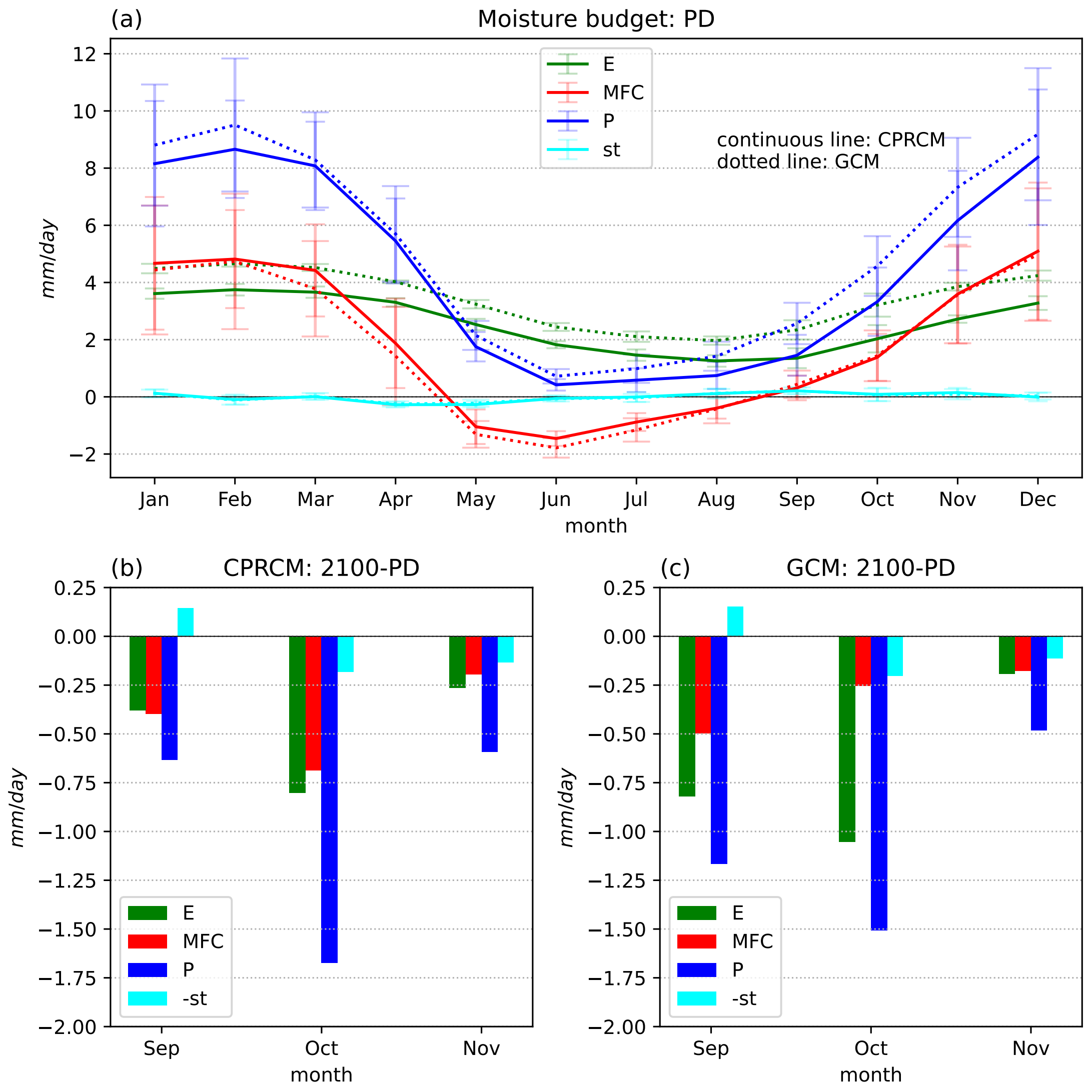

FIG. 6. Moisture budget over CEB. (a) Mean monthly values of daily precipitation (P), evapotranspiration (E), storage term (st), and MFC in CPRCM-PD (solid lines) and GCM-PD (dotted lines). (b) Differences (2100 - PD) of P, E, st, and MFC in the CPRCM. (c) Differences (2100 - PD) of P, E, st, and MFC in the GCM. Error bars in panel a indicate one standard deviation (Wider error bar caps are for the GCM). Statistically significant changes (at 5% level using a two-tailed t-test) are indicated by hatched bars in panels b and c.

that precipitation recycling is an important component of precipitation in central Brazil even in the premonsoon season. CEB region chosen in this study partly overlaps with the regions analyzed in their study and the decline in evapotranspiration is likely to reduce recycling. In addition, studies in other monsoon regions have shown that soil moisture and surface flux gradients aid the progression

Accepted for publication in *Journal of Climate*. DOI 10.1175/JCLI-D-24-0720.1.

of rainfall onset (Menon et al. 2022). The decrease in precipitation during the onset phase in the RCP8.5 scenario can therefore be intensified by the reduction in evapotranspiration. The peak rainy season differs from this in that there is no appreciable change in evapotranspiration, regardless of the increase in precipitation during these months (Supplementary Figures 4,5). This is followed by a more abrupt decline in evapotranspiration at the end of the rainy season in the RCP 8.5 scenario (based on Figure 6a and Supplementary Figure 4).

In general, MFC is positive (indicating convergence of moisture flux, and larger precipitation compared to evapotranspiration) during the peak rainy season (December - March) while it is negative (indicating divergence of moisture flux and larger evapotranspiration compared to precipitation) during the drier months (May - August; Figure 6a for present-day). Between September and November, moisture starts converging over CEB and MFC increases to rainy-season-levels (Figure 6a). However, the MFC differences (2100-PD) are statistically insignificant (using a two tailed t-test) and are either of the same order of (in the CPRCM) or smaller than (in the GCM) the changes in evapotranspiration during the onset phase (see Figure 6b,c for the difference and Supplementary Figure 4 for the MFC in the RCP8.5 scenario). Considering the larger specific humidity in the warmer scenario, this would indicate either a weakening of the atmospheric circulation or a delayed transition from a divergent to convergent circulation. The role of a weakened atmospheric circulation in reducing precipitation was suggested by Vecchi and Soden (2007). Nonetheless, the origin of the anomalous moisture flux divergence is not examined further in the present study, since the changes in MFC are found to be statistically insignificant (still, that does not necessarily imply MFC changes are unimportant), and could be associated with changes in global teleconnections. The subregions also exhibit a similar behaviour with the decline in evapotranspiration being the dominant response during the onset phase (a brief discussion on the moisture budget over the subregions is given in the supplementary file).

Moisture budget analysis provides a glimpse of the prominence of local processes (evapotranspiration) on the hydrological changes during the onset phase over CEB in the CPRCM and GCM simulations. The simulated changes in evapotranspiration is likely related to the changes in either soil water availability or processes that control moisture exchange across the land-atmosphere interface. But, it is challenging to establish a causal relationship between precipitation and evapotranspiration, since the feedback between these two variables is so close. Yet, since vegetation is an

Accepted for publication in *Journal of Climate*. DOI 10.1175/JCLI-D-24-0720.1.

important intermediary in the moisture exchange between land and atmosphere, and as vegetation physiology is sensitive to temperature and atmospheric CO_2 concentration, we expect vegetation to have influenced the surface moisture flux differences between the present-day and future simulations. We test this expectation in the next section.

6. The role of vegetation

In the model, soil water is transferred to the atmosphere via three pathways, canopy evaporation (E_c), bare soil evaporation (E_s) and plant transpiration (E_t). In the JULES land surface scheme, E_s is restricted to the topmost soil layer (layer 1) whereas vegetation can access water from all levels (Folwell et al. 2022). Hence, soil moisture from deeper soil layers interacts with the atmosphere via plant transpiration, which is a function of plant functional types and root density profiles (Best et al. 2011). Figure 7 shows the difference (2100-PD) in E_c and $E_s + E_t$ over CEB and its subregions (since E_s and E_t are not given separately in the model output diagnostics). $E_s + E_t$ dominates the future decline in total evapotranspiration in CEB during the onset of the rainy season. The behaviour is similar in all the subregions, with the WCEB subregion exhibiting the largest decline in $E_s + E_t$ compared to other regions. Although it is impossible to partition this further, we interpret that the decline in these fluxes is primarily due to a reduction in E_t. To test this point, we examine soil moisture-$E_s + E_t$ relationship across soil layers, including the deeper soil layers, where the interaction of soil moisture with the atmosphere is through E_t only (Figure 8 and Table 1).

Figure 8 shows total $E_s + E_t$ as a function of soil moisture in different layers. In general, the decline in $E_s + E_t$ is larger in the regions dominated by broadleaf trees (PFT1; Table 1). For layer 1, the relationship between $E_s + E_t$ and soil moisture is linear and similar in both the present-day and RCP8.5 simulations (Figure 8, first column), although the mean soil moisture content is considerably lower in the RCP8.5 scenario. This behaviour is similar in both the regions dominated by broadleaf trees (PFT1; Figure 8a,i) and in regions where other surface types occupy a significant fraction ("Other", Figure 8e,m). The relationship is approximately linear in soil layers 2 and 3 as well (Figure 8, second and third columns). In regions dominated by broadleaf trees, there is a clear downward shift of the curve indicating that for the same soil moisture content in layers 2 and 3, $E_s + E_t$ has decreased, implying the role of other factors in the reduction of $E_s + E_t$. In other regions, in addition to the decrease in $E_s + E_t$ irrespective of larger moisture availability, the rate at which

Accepted for publication in *Journal of Climate*. DOI 10.1175/JCLI-D-24-0720.1.

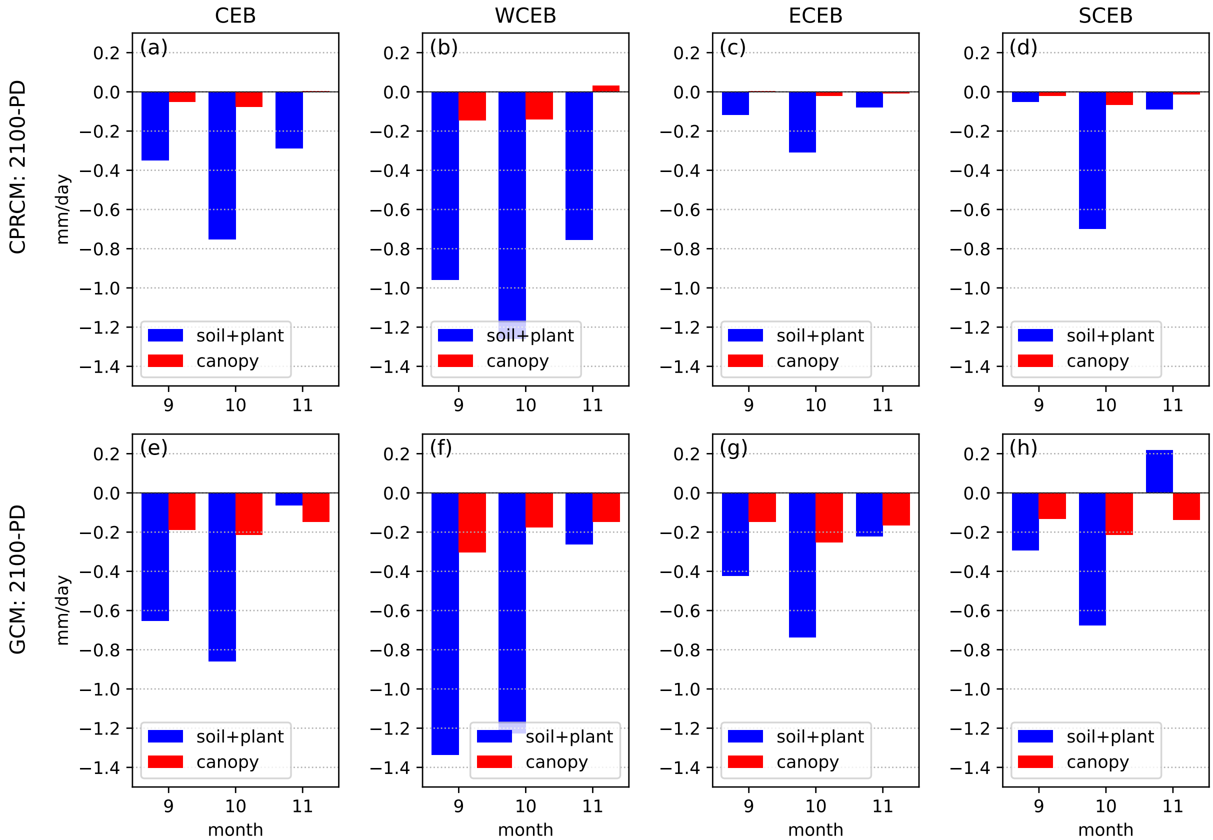

FIG. 7. Differences (2100 - PD) of E_c and $E_s + E_t$ in CEB (first column), WCEB (second column), ECEB (third column), and SCEB (fourth column) from CPRCM (top row) and GCM (bottom row) simulations. Statistically significant changes (at 5% level using a two tailed t-test) are indicated by hatched bars.

$E_s + E_t$ declines with decrease in soil moisture content is also larger. These relationships are less evident in the GCM, especially in the regions dominated by broadleaf trees. For example, $E_s + E_t$ rates in GCM-PD exhibits limited variability with soil moisture content compared to CPRCM-PD or GCM-2100 in regions dominated by broadleaf trees (Figure 8b,j).

Access to the soil moisture in the bottommost soil layer (layer 4), is predominantly by broadleaf trees (Harper et al. 2020). Among all the soil layers, $E_s + E_t$ is least sensitive to soil moisture in this layer during the onset phase. In regions dominated by broadleaf trees, $E_s + E_t$ increases with soil moisture content in CPRCM-PD. However, this relationship is weak in CPRCM-2100 and the larger moisture availability in this layer under the RCP8.5 scenario does not contribute to an increase in $E_s + E_t$ (Figure 8d). The increase in soil moisture content in GCM-2100 (relative

Accepted for publication in *Journal of Climate*. DOI 10.1175/JCLI-D-24-0720.1.

TABLE 1. Climatological mean values of $E_s + E_t$, soil moisture in different soil layers, and subsurface runoff for September to November for areas with broadleaf trees (PFT1) and other vegetation (Others).

Vairable	CPRCM-PD		CPRCM-2100		GCM-PD		GCM-2100	
	PFT1	Other	PFT1	Other	PFT1	Other	PFT1	Other
$E_s + E_t$ (mm/day)	2.5	1.5	1.4	1.2	3	2.1	2	1.7
Soil moisture - Level 1 (kg/m^2)	25.2	11.1	16.7	7.7	33.4	18.3	22.6	11.3
Soil moisture - Level 2 (kg/m^2)	68.5	52.7	64.1	55.2	82.5	59.5	70.6	60.3
Soil moisture - Level 3 (kg/m^2)	169.1	138.3	164.8	151.4	172.1	144.1	171.7	166.3
Soil moisture - Level 4 (kg/m^2)	468.8	475.9	511	513.6	478.5	474.6	483.7	510.9
Subsurface runoff (mm/day)	0.09	0.12	0.09	0.18	0.03	0.05	0.02	0.09

to GCM-PD) is smaller than in the CPRCM. In other regions however, the bottomost layer has larger soil moisture content under the RCP8.5 scenario in both the CPRCM and the GCM. These changes in both the categories may be due to a decline in plant transpiration, although the fractional water utilization from this layer is small in regions dominated by other PFTs. The absence of a linear relationship during the onset phase also makes the attribution less obvious for this layer. Being the bottommost layer in the soil column, layer 4 can also lose water through subsurface runoff. However, the change in subsurface runoff between the present-day and RCP8.5 simulations is quite small (Table 1) and is therefore unlikely to explain the larger soil moisture content in layer 4 under the RCP8.5 scenario. Thus, the decrease in $E_s + E_t$ should at least partly be due to plant physiological changes.

The rate at which plants exchange water through leaves depends on stomatal conductance, which is modelled as a function of photosynthetically active radiation, temperature, vapour pressure deficit, soil moisture content, and atmospheric CO_2 concentration (Collatz et al. 1991, 1992; Cox et al. 1998; Best et al. 2011; Clark et al. 2011). Figure 9 shows the temperature (here, we have chosen daily mean 2m air temperature) dependence of stomatal conductance (daily mean) in the CPRCM (stomatal conductance data is not available from the GCM simulations). A small sub-region is chosen to improve visualization and the choice of the region has negligible impact on the conclusions drawn. In the RCP8.5 scenario, the mean stomatal conductance reduces for all PFTs. The decrease is also evident from the much smaller number of days where stomatal conductance in the RCP8.5 scenario is above the mean value in the present-day. This supports our argument

Accepted for publication in *Journal of Climate.* DOI 10.1175/JCLI-D-24-0720.1.

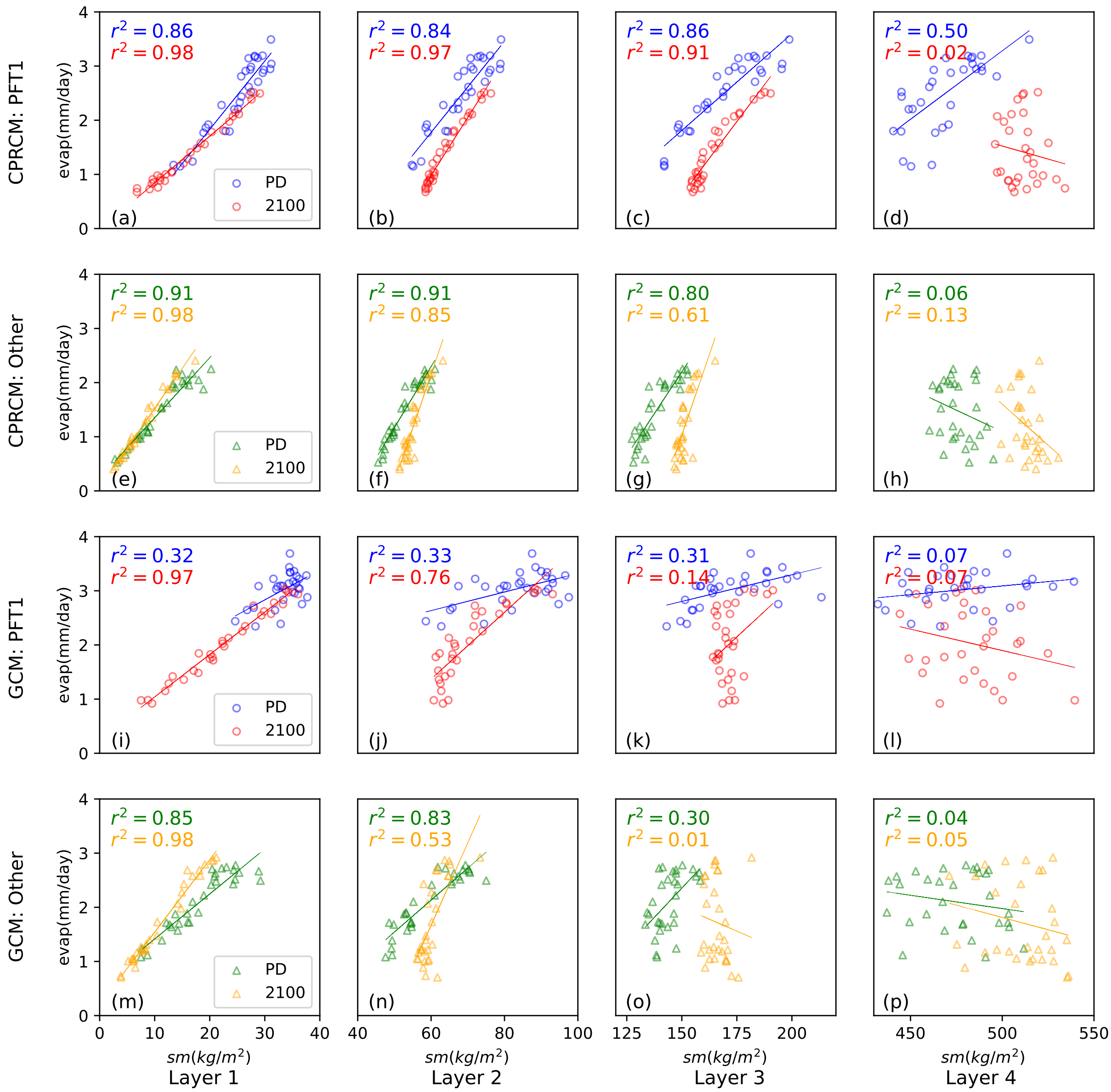

FIG. 8. $E_s + E_t$ (y-axis) as a function of moisture content (x-axis) in different soil layers (Layer 1 - a,e,i,m; Layer 2 - b,f,j,n; Layer 3 - c,g,k,o; Layer 4 - d,h,l,p) in CEB during September to November for the CPRCM (a-h; a-d for PFT1 and e-h for Other) and the GCM (i-p; i-l for PFT1 and m-p for Other). Each dot denotes a monthly value from 10 years of the simulation. PFT1 represents grid cells where broadleaf trees occupy more than 80% of the area and "Other" denotes grid cells in CEB where broadleaf trees are less than 80% (and primarily consisting of C3 and C4 grasses).The lines in each panel represents the linear least squared error fit. The r^2 values between soil moisture and $E_s + E_t$ are also shown in each panel.

Accepted for publication in *Journal of Climate*. DOI 10.1175/JCLI-D-24-0720.1.

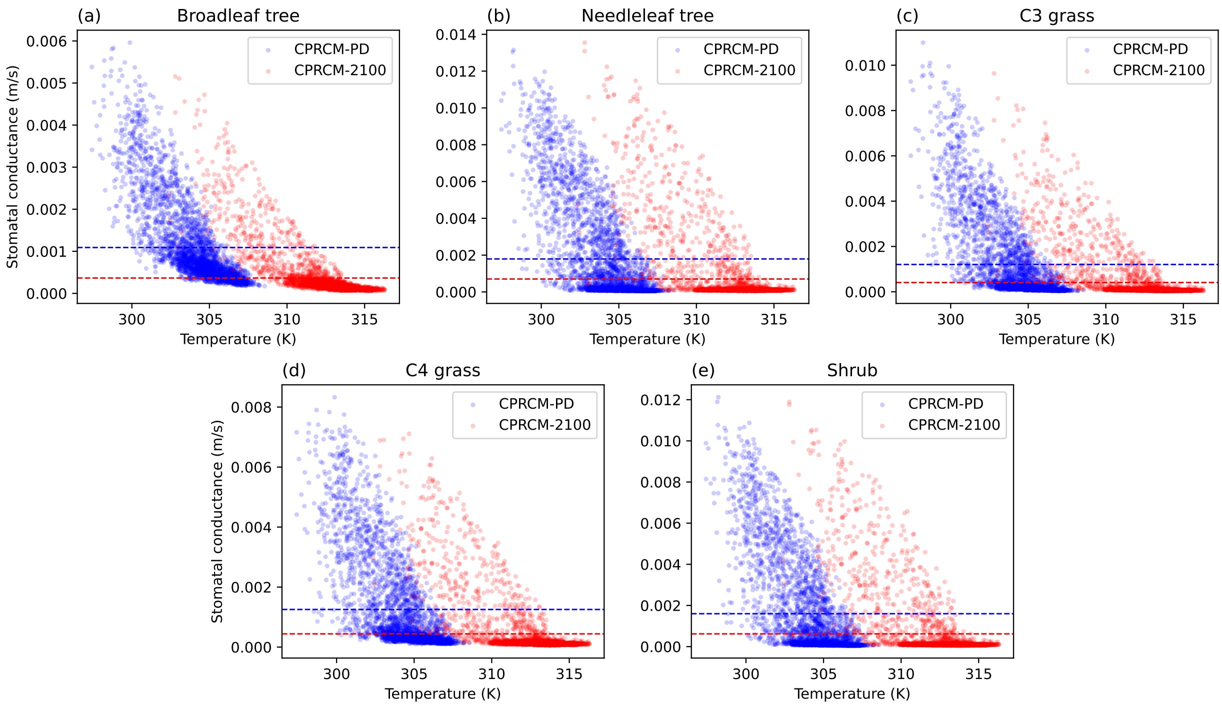

FIG. 9. Relationship between temperature and stomatal conductance (daily mean values) in the CPRCM for the present-day (blue dots) and RCP8.5 (red dots) simulations in a small region within CEB ($-10.25°N$ to $-10°N$, $309.75°E$ to $310°E$) during September to November. Horizontal lines represent the mean value in each case.

that the reduced evapotranspiration is attributable to the changes in plant physiology. The decline in stomatal conductance can be primarily due to two factors, namely, increase in atmospheric CO_2 and increase in temperature, as evidenced by studies using similar land surface parametrizations (Halladay and Good 2017). Daily mean 2m air temperatures are higher by more than 5K in the RCP8.5 scenario (Figure 9). However, other factors like an increase in photosynthetically active radiation due to cloud cover reduction may partially offset the temperature and CO_2 effects.

7. Implications on land-atmosphere coupling

The change in land evaporation affects the surface energy budget and boundary layer characteristics, which would impact the relative roles played by the atmosphere on land and vice versa. To get a grasp on these changes, we employ the coupling index (Dirmeyer 2011; Müller et al. 2021; Baker et al. 2021; Talib et al. 2023), defined as the product of the regression coefficient (β) between two

Accepted for publication in *Journal of Climate*. DOI 10.1175/JCLI-D-24-0720.1.

variables (x, y) and the standard deviation (σ) of the independent variable (x), given below:

$$CI = \beta_{x,y}\sigma_x. \tag{4}$$

This helps identify regions with significant variability in the independent variable and significant sensitivity of the dependent variable to variations in the independent variable simultaneously. For terrestrial coupling index, total soil moisture in the top three layers is chosen as the independent variable (similar to Müller et al. (2021) and since the bottommost soil layer has limited influence on evaporation variability as shown in Figure 8) and land evaporation is chosen as the dependent variable. Similarly, for atmospheric coupling index, land evaporation is chosen as the independent variable and precipitation is chosen as the dependent variable. These choices are based on the interactions that are of interest to this research, namely the dependence of precipitation on soil moisture and vice versa.

Figure 10 shows the monthly terrestrial coupling index for the control simulation from September to November. In CPRCM-PD, evapotranspiration is highly sensitive to soil moisture in most of CEB (especially in WCEB and SCEB) in September and October, similar to the findings of Müller et al. (2021) and Baker et al. (2021). The importance of soil moisture on evapotranspiration in regions with relatively long hydrological memory was also identified by Zanin et al. (2024) (western side of CEB overlaps with their study region). But, since the soil column depth in our simulations is shallower compared to observations, soil moisture memory could be smaller in the simulations in regions with deep-rooted vegetation (Maeda et al. 2017; Zanin 2021). The coupling index decreases in November over CEB along a southwest to northeast direction as the region becomes wetter after the onset of the rainy season. In the RCP8.5 scenario, there is a decline in the terrestrial coupling index in both September and October in parts of CEB. This reduction in sensitivity is rather widespread in October whereas it is concentrated over WCEB in September. The reduced coupling suggests that the region's climate possibly changes from a dry-to-wet transition regime to a rather dry regime during this season in the RCP8.5 scenario. GCM-PD also exhibits significant coupling in the CEB region although the spatial pattern is different compared with CPRCM-PD (Supplementary Figure 9). Over WCEB, CPRCM-PD exhibits stronger coupling in September and October compared to GCM-PD, which is likely due to the larger canopy water contribution to evapotranspiration in the GCM, particularly over dense canopy in WCEB (Folwell et al. 2022).

Accepted for publication in *Journal of Climate*. DOI 10.1175/JCLI-D-24-0720.1.

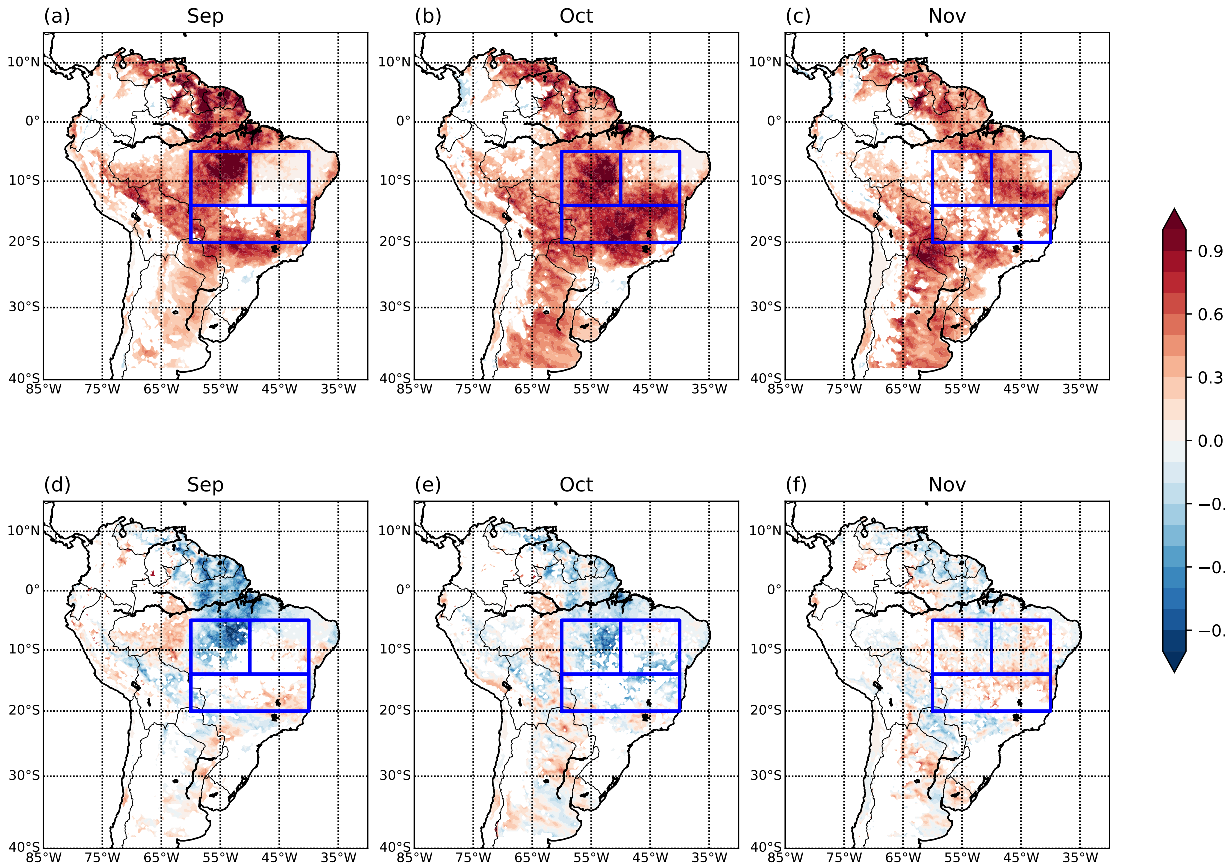

FIG. 10. Terrestrial coupling index (mm/day) during the onset phase in the CPRCM. Top row shows mean values for September, October and November in CPRCM-PD. Bottom row shows the difference (2100 - PD) in terrestrial coupling index. Shades are plotted only where the regression coefficient between soil moisture and evapotranspiration is nonzero at a statistical significance level of 5%. Blue box marks CEB.

The coupling strength is also found to increase over WCEB in GCM-2100, contrary to CPRCM-2100 where the increase is limited to parts of SCEB in September. This is likely due to the different evapotranspiration-soil moisture relationship in GCM-PD and the CPRCM-PD (Figure 8 first column). evapotranspiration in GCM-PD is quite high and exhibits much less variability than in CPRCM-PD, especially in regions dominated by broadleaf trees. In GCM-2100, the increase in the terrestrial coupling index indicates that evapotranspiration becomes more tightly coupled to soil moisture variability, whereas the shift is more subtle in CPRCM-2100.

Accepted for publication in *Journal of Climate.* DOI 10.1175/JCLI-D-24-0720.1.

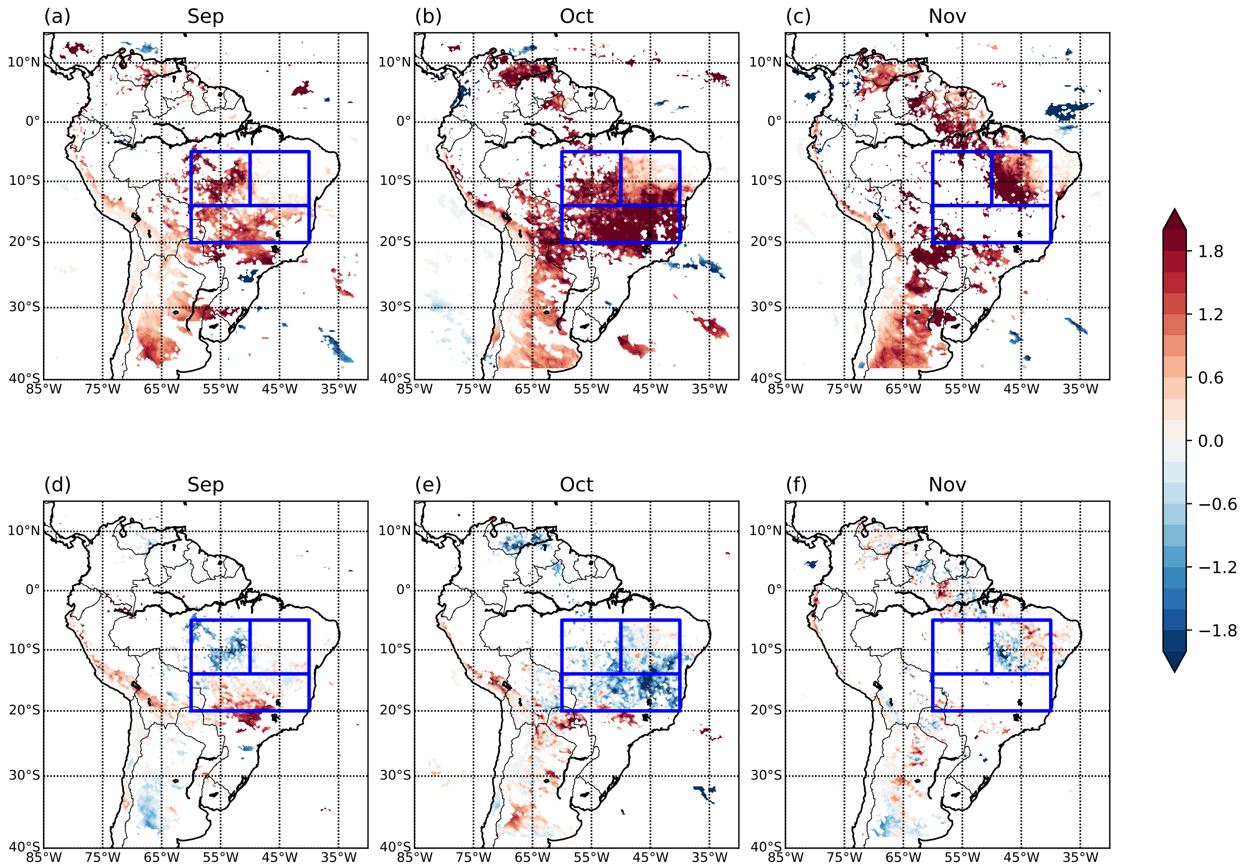

FIG. 11. Atmospheric coupling index (mm/day) during the onset phase in the CPRCM. Top row shows mean values for September, October and November in CPRCM-PD. Bottom row shows the difference (2100 - PD) in atmospheric coupling index. Shades are plotted only where the regression coefficient between evapotranspiration and precipitation is nonzero at a statistical significance level of 5%. Blue box marks CEB.

The atmospheric counterpart of the coupling is shown in Figure 11. In the present-day simulation, the coupling between precipitation and evapotranspiration is the highest in October during the seasonal transition. Significant coupling exists in September as well over a large part of CEB. The regions exhibiting significant sensitivity are confined to the northeastern part of CEB in November. In the RCP8.5 scenario, there is a decline in the atmosphere coupling index in CEB, especially in October. This is consistent with the drying tendency indicated by the terrestrial coupling index which indicates a shift towards a more drier regime. The reduction in plant transpiration may have a significant role here. Studies (e.g., Lintner and Neelin 2009; Collini et al. 2008) have shown

Accepted for publication in *Journal of Climate*. DOI 10.1175/JCLI-D-24-0720.1.

that land moisture supply helps in moistening the atmosphere which preconditions the atmosphere for deep convection. This process might be lacking to some extent in the warmer and drier RCP8.5 scenario, affecting the onset phase rainfall. Regions where strong atmospheric coupling is observed are similar in both CPRCM-PD and GCM-PD (Supplementary Figure 10). However, the coupling is stronger in CPRCM-PD and there are some differences in the future direction of change in October. For instance, over some regions in CEB occupied predominantly by C4 grass, the coupling increases in GCM-2100, while the decline in coupling strength is fairly uniform over CEB in CPRCM-2100.

8. Summary and conclusions

The findings presented here show a significant delay in the onset of SAMS under RCP8.5 scenario. The consensus between two models, one that explicitly resolves convection and one with parametrized convection indicates the robustness of the signal, despite spatial heterogeneity. We diagnose, as found in CMIP6 projections (Bombardi and Boos 2021), that the delay in onset is associated with a delay in the buildup of low-level moist static energy and moisture coupled with enhanced atmospheric stability in the warmer future. This increase in tropospheric stability during the dry to wet transition period, owing to the vertically non-uniform warming signal in the troposphere has the potential to increase convective inhibition during the premonsoon period as shown by Seth et al. (2013). To overcome the enhanced stability, the lower tropospheric moisture content has to increase significantly either via changes in moisture transport or land moisture availability. These increases are seen during the peak rainy season with rainfall unchanged or increasing in the future supported by 30% increases in low-level specific humidity under the RCP8.5 scenario (not shown). This maintenance or increase of moisture is associated with an increase in MFC (Supplementary Figure 5). However, during the onset phase, the decline in evapotranspiration dominates the atmospheric moisture budget (especially in the GCM), although MFC also reduces.

Previous studies have shown that under a warmer scenario, the land, being a finite moisture source, is unable to meet the increase in atmospheric evaporative demand in the dry season which leads to larger land warming (Joshi et al. 2008; Laîné et al. 2014; Byrne and O'Gorman 2016) that amplifies the reduction in relative humidity and enhances dryness. The resulting altered moisture

Accepted for publication in *Journal of Climate*. DOI 10.1175/JCLI-D-24-0720.1.

and dry static energy gradients impact the propensity for convection (Smyth and Ming 2020). We find that, over CEB, evapotranspiration decreases even though the total column soil moisture content increases in the RCP8.5 scenario. This decline is related to reduced transpiration by plants leading to larger soil moisture in the deeper soil layers in the model, whereas the topmost soil layer is consistently drier than that in the present day. Changes in plant physiology associated with temperature changes and increased CO_2 in the RCP8.5 scenario could have played a crucial role here. Stomatal conductance in the land surface model decreases with increased CO_2. The relationship between stomatal conductance and temperature in the model takes the form of a bell-shaped curve, with a drastic reduction in stomatal conductance beyond a temperature threshold (Cox et al. 1998). Parameters controlling these relationships vary across PFTs (Clark et al. 2011). The importance of plant physiological changes for climate projections have been identified in other model studies as well (Halladay and Good 2017; Chadwick et al. 2019; Sikma et al. 2019; Cui et al. 2020). These changes are also found to impact the land-atmosphere coupling in the region during the onset phase.

We also find that the CPRCM simulations provide a similar climate change signal over CEB as the GCM simulations. However, the GCM has a larger lower-tropospheric moisture content and is in general wetter than the CPRCM. The convective parametrization employed in the GCM (Gregory and Rowntree 1990) uses local parcel buoyancy to trigger convection and is known to generate significant amount of light rain due to too frequent convective triggering (Li et al. 2021). This likely explains the larger mean rainfall during the onset phase in the GCM. The future change in the intensity and frequency of precipitation predicted by these models also differs as a result of parametrised versus explicit representation of convection (Kahana et al. 2024).

The results presented also highlight the need to have an accurate representation of plant physiological processes in the land surface model. Plants can acclimatize to changes in environmental conditions to some extent (e.g., Way and Yamori 2014) and incorporating these processes into the land surface model can improve climate projections (Mercado et al. 2018). A recent study by Oliver et al. (2022) found that incorporating thermal acclimation effects on photosynthesis into JULES improved the surface water and carbon fluxes. The current set of experiments does not take into account these aspects which might have some impact on the conclusions drawn. In addition, leaf area index and vegetation cover fraction, which can vary with environmental conditions (Betts

Accepted for publication in *Journal of Climate*. DOI 10.1175/JCLI-D-24-0720.1.

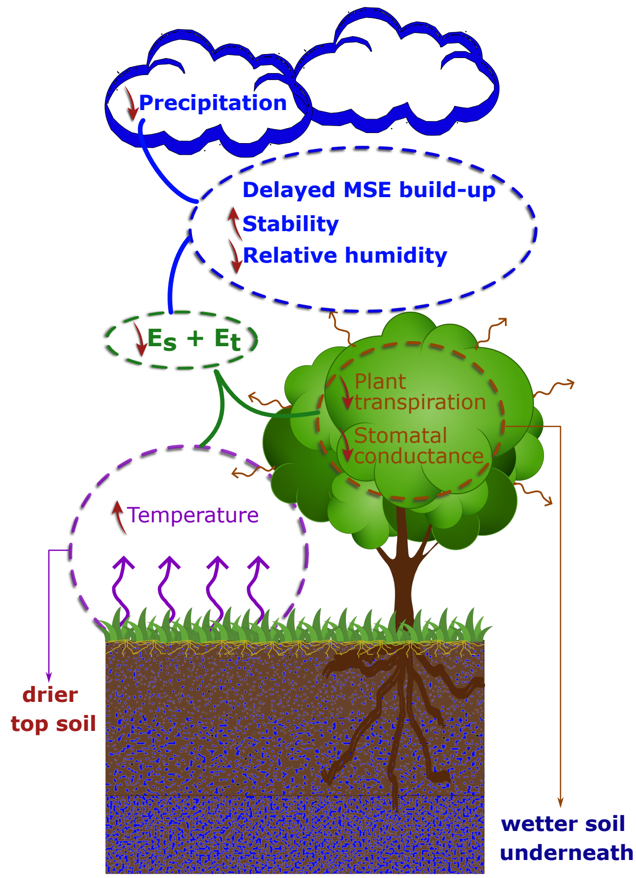

FIG. 12. Schematic of the major factors influencing the delay in rainy season onset over CEB. See text for a description.

et al. 1997; Bala et al. 2006), are also the same across the present-day and RCP8.5 simulations. Simulations in this study may also underestimate soil water utilization by vegetation compared to observations in regions with broadleaf trees. Research in Amazon forests have shown that tree-roots may go to depths of 10m below the soil surface which helps sustain transpiration during the dry season (Jipp et al. 1998; Bruno et al. 2006). Harper et al. (2010) and Zanin (2021) have shown that including this deep-soil water intake modify the simulated energy balance and both dry and wet season characteristics. However, modelling these processes involves significant challenges due to the uncertainties in observations and the diverse nature of the response to climate change in different biomes.

Figure 12 gives a concluding summary of the findings. In a warmer and CO_2 richer scenario, the atmosphere is more stable during the premonsoon phase. Vegetation plays a significant role in

Accepted for publication in *Journal of Climate*. DOI 10.1175/JCLI-D-24-0720.1.

this by regulating the hydrological cycle, which also involves feedback with the atmosphere. The simulated decrease in plant transpiration, as a result of enhanced stomatal closure plus the absence of a significant increase in MFC makes it difficult to overcome the larger atmospheric stability and intensifies the delay in the onset of the rainy season. Here, the bidirectional nature of the interactions between MFC, vegetation, and atmospheric stability cannot be ignored. These findings, despite being based on simulations using a single climate model, have significant implications for land use policies and preparedness in the context of climate change mitigation, given the increasing intensity of droughts in Brazil during recent times (Stríkis et al. 2024) and the detrimental effect on water resources associated with a delayed SAMS onset.

Acknowledgments. This work and its contributors were supported by the Newton Fund through the Met Office Climate Science for Service Partnership Brazil (CSSP Brazil). MTZ and NCGH were also supported by a UKRI Future Leaders Fellowship MR/W011379/1. The authors acknowledge Christopher Taylor and Rebecca Oliver for the useful discussions. The authors would also like to thank the anonymous reviewers for the valuable suggestions.

Data availability statement. The Met Office Unifed Model (UM) CPRCM simulations are available from KH and RK on reasonable request (Halladay et al. 2023).

References

Agudelo, J., J. C. Espinoza, C. Junquas, P. A. Arias, J. P. Sierra, and M. E. Olmo, 2023: Future Projections of Low-Level Atmospheric Circulation Patterns Over South Tropical South America: Impacts on Precipitation and Amazon Dry Season Length. *Journal of Geophysical Research: Atmospheres*, **128 (22)**, e2023JD038 658.

Andrews, T., M. Doutriaux-Boucher, O. Boucher, and P. M. Forster, 2011: A regional and global analysis of carbon dioxide physiological forcing and its impact on climate. *Climate Dynamics*, **36**, 783–792.

Ashfaq, M., and Coauthors, 2021: Robust late twenty-first century shift in the regional monsoons in RegCM-CORDEX simulations. *Climate Dynamics*, **57**, 1463–1488.

Baidya Roy, S., and R. Avissar, 2002: Impact of land use/land cover change on regional hydrometeorology in Amazonia. *Journal of Geophysical Research: Atmospheres*, **107 (D20)**, LBA–4.

Accepted for publication in *Journal of Climate*. DOI 10.1175/JCLI-D-24-0720.1.

Baker, J. C., and Coauthors, 2021: An assessment of land–atmosphere interactions over South America using satellites, reanalysis, and two global climate models. *Journal of Hydrometeorology*, **22 (4)**, 905–922.

Bala, G., K. Caldeira, A. Mirin, M. Wickett, C. Delire, and T. Phillips, 2006: Biogeophysical effects of CO2 fertilization on global climate. *Tellus B: Chemical and Physical Meteorology*, **58 (5)**, 620–627.

Best, M. J., and Coauthors, 2011: The Joint UK Land Environment Simulator (JULES), model description–Part 1: energy and water fluxes. *Geoscientific Model Development*, **4 (3)**, 677–699.

Betts, R. A., P. M. Cox, S. E. Lee, and F. I. Woodward, 1997: Contrasting physiological and structural vegetation feedbacks in climate change simulations. *Nature*, **387 (6635)**, 796–799.

Bombardi, R. J., and W. R. Boos, 2021: Explaining globally inhomogeneous future changes in monsoons using simple moist energy diagnostics. *Journal of Climate*, **34 (21)**, 8615–8634.

Bombardi, R. J., and L. M. Carvalho, 2011: The south atlantic dipole and variations in the characteristics of the south american monsoon in the wcrp-cmip3 multi-model simulations. *Climate Dynamics*, **36**, 2091–2102.

Bombardi, R. J., J. L. Kinter, and O. W. Frauenfeld, 2019: A global gridded dataset of the characteristics of the rainy and dry seasons. *Bulletin of the American Meteorological Society*, **100 (7)**, 1315–1328.

Bombardi, R. J., V. Moron, and J. S. Goodnight, 2020: Detection, variability, and predictability of monsoon onset and withdrawal dates: A review. *International Journal of Climatology*, **40 (2)**, 641–667.

Bottino, M. J., and Coauthors, 2024: Amazon savannization and climate change are projected to increase dry season length and temperature extremes over Brazil. *Scientific Reports*, **14 (1)**, 5131.

Bretherton, C. S., M. E. Peters, and L. E. Back, 2004: Relationships between water vapor path and precipitation over the tropical oceans. *Journal of climate*, **17 (7)**, 1517–1528.

Accepted for publication in *Journal of Climate*. DOI 10.1175/JCLI-D-24-0720.1.

Bruno, R. D., H. R. Da Rocha, H. C. De Freitas, M. L. Goulden, and S. D. Miller, 2006: Soil moisture dynamics in an eastern amazonian tropical forest. *Hydrological Processes: An International Journal*, **20 (12)**, 2477–2489.

Byrne, M. P., and P. A. O'Gorman, 2016: Understanding decreases in land relative humidity with global warming: Conceptual model and GCM simulations. *Journal of Climate*, **29 (24)**, 9045–9061.

Cai, W., and Coauthors, 2021: Changing El Niño–Southern oscillation in a warming climate. *Nature Reviews Earth & Environment*, **2 (9)**, 628–644.

Chadwick, R., D. Ackerley, T. Ogura, and D. Dommenget, 2019: Separating the influences of land warming, the direct CO2 effect, the plant physiological effect, and SST warming on regional precipitation changes. *Journal of Geophysical Research: Atmospheres*, **124 (2)**, 624–640.

Chadwick, R., I. Boutle, and G. Martin, 2013: Spatial patterns of precipitation change in CMIP5: Why the rich do not get richer in the tropics. *Journal of climate*, **26 (11)**, 3803–3822.

Chakraborty, A., R. Nanjundiah, and J. Srinivasan, 2006: Theoretical aspects of the onset of Indian summer monsoon from perturbed orography simulations in a GCM. *Annales Geophysicae*, Copernicus Publications Göttingen, Germany, Vol. 24, 2075–2089.

Chou, C., and J. D. Neelin, 2004: Mechanisms of global warming impacts on regional tropical precipitation. *Journal of climate*, **17 (13)**, 2688–2701.

Chou, C., J. D. Neelin, C.-A. Chen, and J.-Y. Tu, 2009: Evaluating the "rich-get-richer" mechanism in tropical precipitation change under global warming. *Journal of climate*, **22 (8)**, 1982–2005.

Chug, D., F. Dominguez, C. M. Taylor, C. Klein, and S. W. Nesbitt, 2023: Dry-to-wet soil gradients enhance convection and rainfall over subtropical South America. *Journal of Hydrometeorology*, **24 (9)**, 1563–1581.

Clark, D., and Coauthors, 2011: The Joint UK Land Environment Simulator (JULES), model description–Part 2: carbon fluxes and vegetation dynamics. *Geoscientific Model Development*, **4 (3)**, 701–722.

Accepted for publication in *Journal of Climate*. DOI 10.1175/JCLI-D-24-0720.1.

Collatz, G. J., J. T. Ball, C. Grivet, and J. A. Berry, 1991: Physiological and environmental regulation of stomatal conductance, photosynthesis and transpiration: a model that includes a laminar boundary layer. *Agricultural and Forest meteorology*, **54 (2-4)**, 107–136.

Collatz, G. J., M. Ribas-Carbo, and J. A. Berry, 1992: Coupled photosynthesis-stomatal conductance model for leaves of c4 plants. *Functional Plant Biology*, **19 (5)**, 519–538.

Collini, E. A., E. H. Berbery, V. R. Barros, and M. E. Pyle, 2008: How does soil moisture influence the early stages of the South American monsoon? *Journal of Climate*, **21 (2)**, 195–213.

Correa, I. C., P. A. Arias, and M. Rojas, 2021: Evaluation of multiple indices of the South American monsoon. *International Journal of Climatology*, **41**, https://doi.org/10.1002/joc.6880.

Cox, P., C. Huntingford, and R. Harding, 1998: A canopy conductance and photosynthesis model for use in a GCM land surface scheme. *Journal of Hydrology*, **212**, 79–94.

Cui, J., S. Piao, C. Huntingford, X. Wang, X. Lian, A. Chevuturi, A. G. Turner, and G. J. Kooperman, 2020: Vegetation forcing modulates global land monsoon and water resources in a CO2-enriched climate. *Nature communications*, **11 (1)**, 5184.

da Silva, A. E., and L. M. V. de Carvalho, 2007: Large-scale index for South America monsoon (LISAM). *Atmospheric Science Letters*, **8 (2)**, 51–57.

de Oliveira Vieira, S., P. Satyamurty, and R. V. Andreoli, 2013: On the south atlantic convergence zone affecting southern amazonia in austral summer. *Atmospheric Science Letters*, **14 (1)**, 1–6.

Debortoli, N. S., V. Dubreuil, B. Funatsu, F. Delahaye, C. H. De Oliveira, S. Rodrigues-Filho, C. H. Saito, and R. Fetter, 2015: Rainfall patterns in the southern amazon: a chronological perspective (1971–2010). *Climatic Change*, **132 (2)**, 251–264.

Dirmeyer, P. A., 2011: The terrestrial segment of soil moisture–climate coupling. *Geophysical Research Letters*, **38 (16)**.

Dirmeyer, P. A., C. A. Schlosser, and K. L. Brubaker, 2009: Precipitation, recycling, and land memory: An integrated analysis. *Journal of Hydrometeorology*, **10 (1)**, 278–288.

Douville, H., and Coauthors, 2021: Water cycle changes. *Climate Change 2021: The Physical Science Basis. Contribution of Working Group I to the Sixth Assessment Report of the*

Accepted for publication in *Journal of Climate*. DOI 10.1175/JCLI-D-24-0720.1.

Intergovernmental Panel on Climate Change, V. Masson-Delmotte, P. Zhai, A. Pirani, S. Connors, C. Péan, S. Berger, N. Caud, Y. Chen, L. Goldfarb, M. Gomis, M. Huang, K. Leitzell, E. Lonnoy, J. Matthews, T. Maycock, T. Waterfield, O. Yelekçi, R. Yu, and B. Zhou, Eds., Cambridge University Press, book section 8, https://doi.org/10.1017/9781009157896.010, URL https://www.ipcc.ch/report/ar6/wg1/downloads/report/IPCC_AR6_WGI_Chapter08.pdf.

Eltahir, E. A., 1998: A soil moisture–rainfall feedback mechanism: 1. Theory and observations. *Water resources research*, **34 (4)**, 765–776.

Espinoza, J.-C., P. A. Arias, V. Moron, C. Junquas, H. Segura, J. P. Sierra-Pérez, S. Wongchuig, and T. Condom, 2021: Recent changes in the atmospheric circulation patterns during the dry-to-wet transition season in south tropical South America (1979–2020): Impacts on precipitation and fire season. *Journal of Climate*, **34 (22)**, 9025–9042.

Findell, K. L., and E. A. Eltahir, 2003: Atmospheric controls on soil moisture–boundary layer interactions. Part I: Framework development. *Journal of Hydrometeorology*, **4 (3)**, 552–569.

Folwell, S. S., C. M. Taylor, and R. A. Stratton, 2022: Contrasting contributions of surface hydrological pathways in convection permitting and parameterised climate simulations over Africa and their feedbacks on the atmosphere. *Climate Dynamics*, **59 (1)**, 633–648.

Fu, R., and W. Li, 2004: The influence of the land surface on the transition from dry to wet season in Amazonia. *Theoretical and applied climatology*, **78**, 97–110.

Fu, R., B. Zhu, and R. E. Dickinson, 1999: How do atmosphere and land surface influence seasonal changes of convection in the tropical Amazon? *Journal of Climate*, **12 (5)**, 1306–1321.

Fu, R., and Coauthors, 2013: Increased dry-season length over southern Amazonia in recent decades and its implication for future climate projection. *Proceedings of the National Academy of Sciences*, **110 (45)**, 18 110–18 115.

Gan, M. A., V. E. Kousky, and C. F. Ropelewski, 2004: The South America monsoon circulation and its relationship to rainfall over west-central Brazil. *Journal of climate*, **17 (1)**, 47–66.

Gan, M. A., V. B. Rao, and M. C. Moscati, 2005: South American monsoon indices. *Atmospheric Science Letters*, **6 (4)**, 219–223.

Accepted for publication in *Journal of Climate*. DOI 10.1175/JCLI-D-24-0720.1.

Gash, J., and C. Nobre, 1997: Climatic effects of Amazonian deforestation: Some results from ABRACOS. *Bulletin of the American meteorological society*, **78 (5)**, 823–830.

Gregory, D., and P. Rowntree, 1990: A mass flux convection scheme with representation of cloud ensemble characteristics and stability-dependent closure. *Monthly Weather Review*, **118 (7)**, 1483–1506.

Haghtalab, N., N. Moore, B. P. Heerspink, and D. W. Hyndman, 2020: Evaluating spatial patterns in precipitation trends across the amazon basin driven by land cover and global scale forcings. *Theoretical and Applied Climatology*, **140 (1)**, 411–427.

Halladay, K., and P. Good, 2017: Non-linear interactions between CO2 radiative and physiological effects on Amazonian evapotranspiration in an Earth system model. *Climate Dynamics*, **49 (7)**, 2471–2490.

Halladay, K., R. Kahana, B. Johnson, C. Still, G. Fosser, and L. Alves, 2023: Convection-permitting climate simulations for South America with the Met Office Unified Model. *Climate Dynamics*, **61 (11)**, 5247–5269.

Harper, A. B., A. S. Denning, I. T. Baker, M. D. Branson, L. Prihodko, and D. A. Randall, 2010: Role of deep soil moisture in modulating climate in the amazon rainforest. *Geophysical Research Letters*, **37 (5)**.

Harper, A. B., and Coauthors, 2020: Improvement of modelling plant responses to low soil moisture in JULESvn4. 9 and evaluation against flux tower measurements. *Geoscientific Model Development Discussions*, **2020**, 1–42.

Hersbach, H., and Coauthors, 2020: The era5 global reanalysis. *Quarterly journal of the royal meteorological society*, **146 (730)**, 1999–2049.

Hofmann, G. S., and Coauthors, 2023: Changes in atmospheric circulation and evapotranspiration are reducing rainfall in the brazilian cerrado. *Scientific Reports*, **13 (1)**, 11 236.

Hohenegger, C., P. Brockhaus, C. S. Bretherton, and C. Schär, 2009: The soil moisture–precipitation feedback in simulations with explicit and parameterized convection. *Journal of Climate*, **22 (19)**, 5003–5020.

Accepted for publication in *Journal of Climate*. DOI 10.1175/JCLI-D-24-0720.1.

Huffman, G. J., E. Stocker, D. Bolvin, E. Nelkin, and J. Tan, 2024: Gpm imerg final precipitation l3 1 day 0.1 degree x 0.1 degree v07. *Goddard Earth Sciences Data and Information Services Center (GES DISC)*.

Jia, G., and Coauthors, 2019: Land–climate interactions. *Climate Change and Land: an IPCC special report on climate change, desertification, land degradation, sustainable land management, food security, and greenhouse gas fluxes in terrestrial ecosystems*, P. Shukla, J. Skea, E. C. Buendia, V. Masson-Delmotte, H.-O. Pörtner, D. Roberts, P. Zhai, R. Slade, S. Connors, R. van Diemen, M. Ferrat, E. Haughey, S. Luz, S. Neogi, M. Pathak, J. Petzold, J. P. Pereira, P. Vyas, E. Huntley, K. Kissick, M. Belkacemi, and J. Malley, Eds.

Jipp, P. H., D. C. Nepstad, D. Cassel, and C. Reis de Carvalho, 1998: Deep soil moisture storage and transpiration in forests and pastures of seasonally-dry amazonia. *Climatic change*, **39 (2)**, 395–412.

Joshi, M. M., J. M. Gregory, M. J. Webb, D. M. Sexton, and T. C. Johns, 2008: Mechanisms for the land/sea warming contrast exhibited by simulations of climate change. *Climate dynamics*, **30**, 455–465.

Kahana, R., K. Halladay, L. M. Alves, R. Chadwick, and A. J. Hartley, 2024: Future precipitation projections for Brazil and tropical South America from a Convection-permitting climate simulation. *Frontiers*, **6**, https://doi.org/10.3389/fclim.2024.1419704.

Kendon, E. J., N. M. Roberts, C. A. Senior, and M. J. Roberts, 2012: Realism of rainfall in a very high-resolution regional climate model. *Journal of Climate*, **25 (17)**, 5791–5806.

Kodama, Y., 1992: Large-scale common features of subtropical precipitation zones (the Baiu frontal zone, the SPCZ, and the SACZ) Part I: Characteristics of subtropical frontal zones. *Journal of the Meteorological Society of Japan. Ser. II*, **70 (4)**, 813–836.

Koster, R. D., and Coauthors, 2004: Regions of strong coupling between soil moisture and precipitation. *Science*, **305 (5687)**, 1138–1140.

Kousky, V. E., 1988: Pentad Outgoing Longwave Radiation Climatology for the South American Sector. *Revista Brasileira de Meteorologia*, **3**, 217–231.

Accepted for publication in *Journal of Climate*. DOI 10.1175/JCLI-D-24-0720.1.

Laîné, A., H. Nakamura, K. Nishii, and T. Miyasaka, 2014: A diagnostic study of future evaporation changes projected in CMIP5 climate models. *Climate Dynamics*, **42**, 2745–2761.

Li, P., K. Furtado, T. Zhou, H. Chen, and J. Li, 2021: Convection-permitting modelling improves simulated precipitation over the central and eastern Tibetan Plateau. *Quarterly Journal of the Royal Meteorological Society*, **147 (734)**, 341–362.

Liebmann, B., S. J. Camargo, A. Seth, J. A. Marengo, L. M. Carvalho, D. Allured, R. Fu, and C. S. Vera, 2007: Onset and end of the rainy season in South America in observations and the ECHAM 4.5 atmospheric general circulation model. *Journal of Climate*, **20 (10)**, 2037–2050.

Lintner, B. R., and J. D. Neelin, 2009: Soil moisture impacts on convective margins. *Journal of Hydrometeorology*, **10 (4)**, 1026–1039.

Ma, J., R. Chadwick, K.-H. Seo, C. Dong, G. Huang, G. R. Foltz, and J. H. Jiang, 2018: Responses of the tropical atmospheric circulation to climate change and connection to the hydrological cycle. *Annual Review of Earth and Planetary Sciences*, **46 (1)**, 549–580.

Maeda, E. E., X. Ma, F. H. Wagner, H. Kim, T. Oki, D. Eamus, and A. Huete, 2017: Evapotranspiration seasonality across the amazon basin. *Earth System Dynamics*, **8 (2)**, 439–454.

Marengo, J. A., J. C. Jimenez, J.-C. Espinoza, A. P. Cunha, and L. E. Aragão, 2022: Increased climate pressure on the agricultural frontier in the eastern amazonia–cerrado transition zone. *Scientific reports*, **12 (1)**, 457.

Marengo, J. A., and Coauthors, 2012: Recent developments on the South American monsoon system. *International Journal of Climatology*, **32 (1)**, 1–21.

Martinez, J. A., and F. Dominguez, 2014: Sources of atmospheric moisture for the La Plata River basin. *Journal of Climate*, **27 (17)**, 6737–6753.

Menon, A., A. G. Turner, A. Volonté, C. M. Taylor, S. Webster, and G. Martin, 2022: The role of mid-tropospheric moistening and land-surface wetting in the progression of the 2016 Indian monsoon. *Quarterly Journal of the Royal Meteorological Society*, **148 (747)**, 3033–3055.

Accepted for publication in *Journal of Climate*. DOI 10.1175/JCLI-D-24-0720.1.

Mercado, L. M., and Coauthors, 2018: Large sensitivity in land carbon storage due to geographical and temporal variation in the thermal response of photosynthetic capacity. *New Phytologist*, **218 (4)**, 1462–1477.

Miralles, D. G., P. Gentine, S. I. Seneviratne, and A. J. Teuling, 2019: Land–atmospheric feedbacks during droughts and heatwaves: state of the science and current challenges. *Annals of the New York Academy of Sciences*, **1436 (1)**, 19–35.

Moon, S., and K.-J. Ha, 2020: Future changes in monsoon duration and precipitation using CMIP6. *npj Climate and Atmospheric Science*, **3 (1)**, 45.

Müller, O. V., P. L. Vidale, B. Vannière, R. Schiemann, R. Senan, R. J. Haarsma, and J. H. Jungclaus, 2021: Land–atmosphere coupling sensitivity to GCMs resolution: A multimodel assessment of local and remote processes in the Sahel hot spot. *Journal of Climate*, **34 (3)**, 967–985.

Nieto-Ferreira, R., T. M. Rickenbach, and E. A. Wright, 2011: The role of cold fronts in the onset of the monsoon season in the South Atlantic convergence zone. *Quarterly Journal of the Royal Meteorological Society*, **137 (657)**, 908–922.

Nworgu, U. C., H. C. Nnamchi, and N. E. Rosário, 2024: Divergent future change in south atlantic ocean dipole impacts on regional rainfall in cmip6 models. *Environmental Research: Climate*, **3 (3)**, 035 002.

Oliver, R. J., and Coauthors, 2022: Improved representation of plant physiology in the JULES-vn5. 6 land surface model: photosynthesis, stomatal conductance and thermal acclimation. *Geoscientific Model Development Discussions*, **2022**, 1–41.

Prein, A. F., and Coauthors, 2015: A review on regional convection-permitting climate modeling: Demonstrations, prospects, and challenges. *Reviews of geophysics*, **53 (2)**, 323–361.

Raia, A., and I. F. A. Cavalcanti, 2008: The life cycle of the South American monsoon system. *Journal of Climate*, **21 (23)**, 6227–6246.

Reynolds, R. W., T. M. Smith, C. Liu, D. B. Chelton, K. S. Casey, and M. G. Schlax, 2007: Daily High-Resolution-Blended Analyses for Sea Surface Temperature. *Journal of Climate*, **20**, 5473–5496, https://doi.org/10.1175/2007JCLI1824.1.

Accepted for publication in *Journal of Climate*. DOI 10.1175/JCLI-D-24-0720.1.

Rowell, D. P., and S. Berthou, 2023: Fine-Scale Climate Projections: What Additional Fixed Spatial Detail Is Provided by a Convection-Permitting Model? *Journal of Climate*, **36 (4)**, 1229–1246.

Seager, R., M. Cane, N. Henderson, D.-E. Lee, R. Abernathey, and H. Zhang, 2019: Strengthening tropical Pacific zonal sea surface temperature gradient consistent with rising greenhouse gases. *Nature Climate Change*, **9 (7)**, 517–522.

Seth, A., S. A. Rauscher, M. Biasutti, A. Giannini, S. J. Camargo, and M. Rojas, 2013: CMIP5 projected changes in the annual cycle of precipitation in monsoon regions. *Journal of climate*, **26 (19)**, 7328–7351.

Sikma, M., J. Vilà-Guerau de Arellano, X. Pedruzo-Bagazgoitia, T. Voskamp, B. Heusinkveld, N. Anten, and J. Evers, 2019: Impact of future warming and enhanced [co2] on the vegetation-cloud interaction. *Journal of Geophysical Research: Atmospheres*, **124 (23)**, 12 444–12 454.

Smyth, J. E., and Y. Ming, 2020: Characterizing drying in the South American monsoon onset season with the moist static energy budget. *Journal of Climate*, **33 (22)**, 9735–9748.

Smyth, J. E., and Y. Ming, 2021: Investigating the impact of land surface characteristics on monsoon dynamics with idealized model simulations and theories. *Journal of Climate*, **34 (19)**, 7943–7958.

Stratton, R. A., and Coauthors, 2018: A Pan-African convection-permitting regional climate simulation with the met office unified model: CP4-Africa. *Journal of Climate*, **31 (9)**, 3485–3508.

Stríkis, N. M., and Coauthors, 2024: Modern anthropogenic drought in Central Brazil unprecedented during last 700 years. *Nature communications*, **15 (1)**, 1728.

Talamoni, I. L., I. F. Cavalcanti, P. Y. Kubota, D. C. de Souza, J. C. Baker, and R. M. Vieira, 2022: Surface and atmospheric patterns for early and late rainy season onset years in South America. *Climate Dynamics*, **59 (9)**, 2815–2830.

Talib, J., O. V. Müller, E. J. Barton, C. M. Taylor, and P. L. Vidale, 2023: The representation of soil moisture-atmosphere feedbacks across the Tibetan Plateau in CMIP6. *Advances in Atmospheric Sciences*, **40 (11)**, 2063–2081.

Accepted for publication in *Journal of Climate*. DOI 10.1175/JCLI-D-24-0720.1.

Taylor, C. M., C. E. Birch, D. J. Parker, N. Dixon, F. Guichard, G. Nikulin, and G. M. Lister, 2013: Modeling soil moisture-precipitation feedback in the Sahel: Importance of spatial scale versus convective parameterization. *Geophysical Research Letters*, **40 (23)**, 6213–6218.

Thome Sena, A. C., and G. Magnusdottir, 2020: Projected end-of-century changes in the South American Monsoon in the CESM large ensemble. *Journal of Climate*, **33 (18)**, 7859–7874.

Vecchi, G. A., and B. J. Soden, 2007: Global warming and the weakening of the tropical circulation. *Journal of Climate*, **20 (17)**, 4316–4340.

Vera, C., and Coauthors, 2006: Toward a unified view of the American monsoon systems. *Journal of climate*, **19 (20)**, 4977–5000.

Way, D. A., and W. Yamori, 2014: Thermal acclimation of photosynthesis: on the importance of adjusting our definitions and accounting for thermal acclimation of respiration. *Photosynthesis research*, **119**, 89–100.

Wei, J., and P. A. Dirmeyer, 2012: Dissecting soil moisture-precipitation coupling. *Geophysical Research Letters*, **39 (19)**.

Wright, J. S., R. Fu, J. R. Worden, S. Chakraborty, N. E. Clinton, C. Risi, Y. Sun, and L. Yin, 2017: Rainforest-initiated wet season onset over the southern Amazon. *Proceedings of the National Academy of Sciences*, **114 (32)**, 8481–8486.

Xue, Y., F. De Sales, W. Li, C. Mechoso, C. Nobre, and H. Juang, 2006: Role of land surface processes in South American monsoon development. *Journal of climate*, **19 (5)**, 741–762.

Zanin, P. R., 2021: Soil water uptake by amazonian trees and simulation of impacts on energy fluxes and soil moisture dynamics at the LBA flux towers. *Revista Brasileira de Meteorologia*, **36 (3)**, 441–454.

Zanin, P. R., D. Pareja-Quispe, and J.-C. Espinoza, 2024: Evapotranspiration in the amazon basin: Couplings, hydrological memory and water feedback. *Agricultural and Forest Meteorology*, **352**, 110 040.

Zanin, P. R., and P. Satyamurty, 2021: Interseasonal and interbasins hydrological coupling in South America. *Journal of Hydrometeorology*, **22 (6)**, 1609–1625.

Accepted for publication in *Journal of Climate*. DOI 10.1175/JCLI-D-24-0720.1.

Zemp, D., C.-F. Schleussner, H. Barbosa, R. Van der Ent, J. F. Donges, J. Heinke, G. Sampaio, and A. Rammig, 2014: On the importance of cascading moisture recycling in South America. *Atmospheric Chemistry and Physics*, **14 (23)**, 13 337–13 359.

Zilli, M. T., and Coauthors, 2024: The added value of using convective-permitting regional climate model simulations to represent cloud band events over South America. *Climate Dynamics*, **62**, 10 543—-10 564.

Accepted for publication in *Journal of Climate*. DOI 10.1175/JCLI-D-24-0720.1.